POLITECNICO DI TORINO

Department of Mechanical and Aerospace Engineering

Masters's degree in

Automotive Engineering

Master Thesis

Definition and Vibration Monitoring of the Endurance Test for an e-Axle

Supervisor:
Prof. Enrico Galvagno

Candidate:
Giorgio De Donno

Company Tutors:
Eng. Domenico Netti
Eng. Vincenzo Rombolà

ACADEMIC YEAR 2022 - 2023

Abstract

The development of e-Drive transmissions has brought about a revolution in the product validation process, requiring new testing solutions to face new challenges in identifying and correcting any vulnerabilities. Electric vehicles usually have a single speed ratio between input and output sufficient to cover the entire speed range required, with electric motors capable of reaching rotational speeds even higher than 18000 rpm and with rather high transmission ratios. With reference to heavy-duty vehicle applications, characterized by speeds up to 120 km/h and high torque required at the wheels, this means that the torque transformation between the transmission input shaft and the output shaft is significant, even up to a factor of 25. This high speed - high torque combination represents a major challenge for the design of these components, since these conditions can cause more frequent damage in rotating parts that have surfaces in relative contact, such as rolling bearings and gears.

The present thesis work, conducted in FPT Industrial S.p.A., is devoted to the definition of an endurance test for an e-Axle for battery-electric (BEV) and fuel cell electric (FCEV) heavy-duty trucks and the application of some vibration monitoring techniques, with the aim of detecting an early damage in the gearbox during the test. Data analysis of some vehicular mission on different routes, allowed to extract a duty cycle equivalent in terms of fatigue damage to the typical customer vehicle mileage, that is used to define the endurance test bench cycle. Subsequently, the operating conditions of the e-Axle during the test were monitored with vibration analysis. The study focused on implementing a method to identify a damaged component before it fails, allowing it to be replaced in time, saving time and money, as a sudden failure of an e-Axle component during the test could lead to its complete and permanent damage. Vibration monitoring was conducted on two levels of analysis in parallel. The first, based on different vibration indicators, makes it possible to identify any sudden changes in the operating conditions of the e-Axle and to follow the progress of the test over time. While the second allows for a more detailed analysis, focusing on rolling bearing fault detection. In order to isolate only the useful contribution for the detection of bearings vibrational signature, an algorithm has been implemented in *MATLAB®* able to separate it from the overall noise and to identify, through frequency analysis, the possible presence of a defect and its location from the characteristic frequencies.

Nomenclature

Acronym	Full name
BPFI	Ball Pass Frequency Inner ring
BPFO	Ball Pass Frequency Outer ring
BSF	Ball Spin Frequency
COT	Computed Order Tracking
EA	Envelope Analysis
FTF	Fundamental train frequency
FK	Fast Kurtogram
GMF	Gear Mesh Frequency
IEPC	Integrated Electric Powertrain Component
SA	Synchronous Average
SK	Spectral Kurtosis
TSA	Time Synchronous Average
UUT	Unit Under Test

Table of contents

1. Introduction

1.1. Scope of the thesis

The important technological change that the transport sector is experiencing has led vehicle manufacturers to electrify propulsion systems, with the aim of reducing global emissions. Computer simulations, made with virtual models, allow to represent the functioning modes of the component in an ever more faithful way to reality and therefore to optimize the design in the prototypal phase, however the durability tests remain essential to validate the successful design.

The aim of this thesis is the definition of an endurance test for an e-Axle for heavy-duty BEV and FCEV applications and the monitoring of its conditions during the bench test run with vibration analysis. To validate all mechanical components of the e-Axle against fatigue damage, a durability test must be performed. Due to the obvious impossibility of replicating the entire vehicle life in terms of mileage, which in the case of industrial vehicles can exceeds 1 000 000 km, an accelerated test was studied on the test bench, which would allow to verify in equi-damage all the mechanical components of the e-Axle. Starting from the analysis of some real vehicular mission data on various routes, a duty cycle equivalent to the typical vehicle mileage of a customer was obtained, and then extended to the target in terms of mileage to be validated. Using the Palmgren-Miner theory on the study of the accumulation of fatigue damage, an equivalent test cycle was defined with two load blocks which, repeated a certain number of times, would allow to obtain the same number of damage of the duty cycle. Once the test cycle was defined, attention was focused on monitoring the operating conditions of the e-Axle during the test. Since a fault of some mechanical component during the test could cause significant and permanent damage to the entire e-Axle, the vibration monitoring of the components allows to identify an early failure and replace the defective component before having a catastrophic result. The study focused on identifying and implementing a reliable method for monitoring the state of health of the machine, selecting among those in the literature. In particular, two types of analyses were conducted. A first-level one, allows to have a macro view of the progress of the test over time, monitoring different vibration features, with the aim of identifying any changes in the operating status. The second one made it possible to carry out a more in-depth analysis, with the specific aim of identifying a localized damage in rolling element

bearings. To address this need, the attention was focused on finding and implementing in *MATLAB®*, a method that would allow to extract the necessary information hidden within the accelerometric signal.

In the following report, all sensitive data owned by the company in which I carried out the thesis have been omitted or obscured. For this reason, in this public version, some tables or charts do not contain numeric values. The full version is available upon request, in agreement with the company.

1.2. e-Axle overview

In the following section it's provided a general overview of the characteristics and the layout of the e-Axle that has been analyzed in this thesis. It is an e-Drive transmission designed by the FPT Industrial company for heavy-duty truck applications with a Gross Vehicle Weight (GVW) up to 44 tons. It is an Integrated Electric Powertrain Component (IEPC), means a combined system of 2 electric motors together with the functionality of single speed gearbox with a total gear ratio of 25. It has been developed for applications on Battery Electric Vehicles (BEV), with a declared useful life of up to 1 200 000 km. The design fully integrates all the mechanical and electrical components in a compact solution that is capable to deliver 840 kW of peak power and a 45 kNm of maximum wheel torque. (1) Below are shown some images for illustrative purposes.

Figure 1: e-Axle overview (images courtesy of FPT Industrial (1))

2. Endurance test

The reliability test of automotive powertrain system is an important measure to evaluate and verify the durability of powertrain. For this purpose, the automotive powertrain's parts industries have adopted rig testing technology since the 1980s. (2)

In the design and development of powertrain for industrial vehicles, there are always certain objectives regarding vehicle speed, acceleration, weight and energy saving to achieve. Among these goals, it is of extreme importance to survey the endurance capacity of the drivetrain. To replicate fatigue damage and failure modes that can occur during the lifetime of the product, an accelerated durability test is developed in the dynamometer cell, with the aim to reduce testing time and simulate road tests at the test rig. In addition to driveline endurance tests, components interaction during operation can be investigated for a wide variety of simulated driving conditions. (3)

A detailed damage analysis is needed to correlate the road test to a bench test, therefore a precise representation of the powertrain road load test is essential for durability test development at the test rig. Usually, the loads are determined either with vehicle measurements or with simulations, for example at the early stages of product development.

The loading spectra can be measured by driving an instrumented vehicle over different predefined test tracks with various test vehicles. The vehicle is equipped with non-contact torque telemeter to measure the shaft torque and sensors for rotation speed and other vehicle parameters, such as temperature and displacement of different components. Next, torque and speed data collected are compressed into block loading spectrum based on fatigue damage equivalent principle, thus achieving the drivetrain testing life equivalent to the customers' usage profile.

A typical test schedule combines several mixed variables, considering the road category (highway, country route, urban route), the vehicle speed, the traffic condition, the traveling distance on different route, the different payload of the vehicle and the region where the test is performed. The loading profile of the vehicle is affected by the driver variability, but also by the road roughness and the weather conditions that influence the friction coefficient between tire and ground. In order to take into account all these variables, the loading measurements of different tests have to be processed to extrapolate the loading histories of an equivalent duty cycle representative of the typical vehicle life.

2.1. Test rig vs test track

Performing most dynamic tests in the test cell rather than on a test track has a number of advantages, some of them are listed below:

- Any desired load and speed profile can be run on the test rig, obviously in the limit of the dynamometer, without any constraint given by the road condition.
- The test rig allows the use of instrumentation that cannot be installed directly on the vehicle, also for the impossibility to reach all the locations where the components are installed.
- The entire test sequence can be automated with the use of actuators that can operate the gear shift lever, the pedals and the clutch (where required). This results in a considerable operating cost reduction.
- It is not required a complete vehicle. This is essential at the early stages of product development, when still all the components are not available or the vehicle may not be available as final design.
- Synthetic load profiles, such as in accelerated durability tests save a lot of time.
- High degree of reproducibility of individual experiment sequences.

2.2. Method to derive the test cycle

The proposed approach for testing drive components of the e-Axle is based on the road load data collected on the vehicle under consideration. These data are representative of the duty cycle that the different mechanical subcomponents have to withstand during the vehicle life.

The accelerated test cycle is derived from the analysis of these data based on Miner's equi-damage principle and Weibull's theory for reliability study.

2.2.1. Cycle counting methods

The linear fatigue damage model indicate that the fatigue damage is directly associated with the cycle ratio n_i / N_i where n_i is the number of applied stress cycles and N_i is the fatigue life at a precise level of stress amplitude. In order to determine the basic fatigue data, we need to refer to the material properties produced by the constant amplitude stress test, while different methods can be used to determine the number of stress cycles applied to the component.

Typically, the amplitude of the loading is not constant, but changes with time, so cycles have to be counted using time histories of the loading parameter of interest, such as force, torque, stress, strain, acceleration or deflection. One complete stress cycle in a time domain is related to a closed hysteresis loop in the local stress-strain coordinate and consists of two phases respectively of loading and unloading. (4)

The mechanical components of the drivetrain that are subjected to fatigue damage are gears, bearings and shafts. A gear set fatigue damage is related to the loading cycle applied on the teeth subjected to an alternated bending moment for several cycles. It is evident that the loading cycles applied on each tooth is directly related to the torque applied on the related shaft and to its number of revolutions.

The techniques used to extract the number of cycles with the corresponding stress amplitude from load-time histories can be the one-parameter cycle counting methods known with the names of *level-crossing, peak-valley* and *range counting* or two-parameter method such as the *rainflow counting* method. For our analysis, a range counting method was considered, where the amount of load in the load time history had to be divided into a series of torque levels, ordered from highest to lowest, choosing a discretization of the torque intervals. In each cluster correspondent to a stress level are reported the number of cycles, referred to a shaft, usually the input or the output shaft of the transmission, completed at that torque range.

To extract the number of cycles, it is necessary to acquire simultaneously the rotational speed of the wheels and the applied torque with a fixed and equal sampling rate. The number of cycles of the reference shaft n_i are defined as follows and are computed for each time instant of the loading history.

$$n_i = \sum_{i=1}^{k} \int_{\Delta t_i} RPM(t)\, dt$$

where $RPM(t)$ is the speed and Δt_i are the discrete time intervals at which data acquisition is performed. It is important to specify that to allow a fair comparison between different test acquisitions, it is necessary to carry out the analysis with the same discretization of the torque levels for all.

Rotating Moment Histogram (RMH) is a type of diagram usually used to get a representation of the load history as a function of the number of shaft cycles, an example is shown in Figure 1. The *x-axis* is a log scale of the number of shaft revolutions and on the *y-axis* there are the torque levels. The points on the graph represents a certain number of revolutions at a specific torque level. In Figure 1, the positive and negative torque represents the torque applied by the propeller shaft in the drive and coast phases.

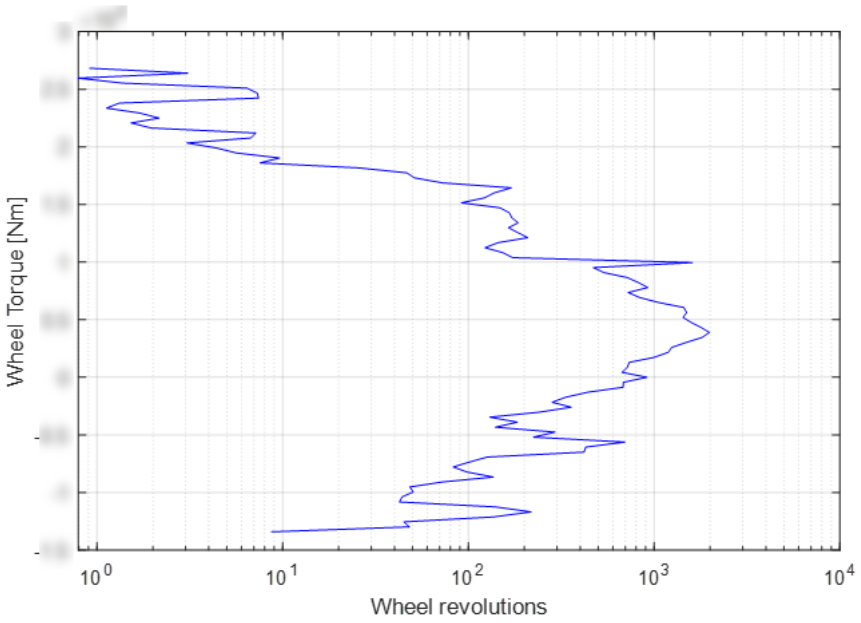

Figure 2: Rotating Moment Histogram (RMH)

2.2.2. Cycles extrapolation

To perform damage analysis, it is necessary to extrapolate the recorded load history of the duty cycle for a much longer time period, usually the vehicle life target mileage. One traditional technique is to set up a *cumulative exceedance diagram* that is based on the short-term measurement and to extrapolate the cycles and load levels for the target life. The cumulative exceedance cycles are generated for each torque level accumulating the cycles starting from the maximum and minimum load level up to zero. It represents a simple way to visualize the envelope of the loading spectrum. The long-term loading spectrum can be generated by shifting the cumulative exceedance diagram rightward to higher cycles by an extrapolation factor. In Figure 2 it is represented an example of this diagram, also called cumulative Load – Cycles and the corresponding extrapolated loading spectrum for a higher number of cycles. The *x-axis* is a log scale of the number of cumulative wheel revolutions and on the *y-axis* there are the torque levels.

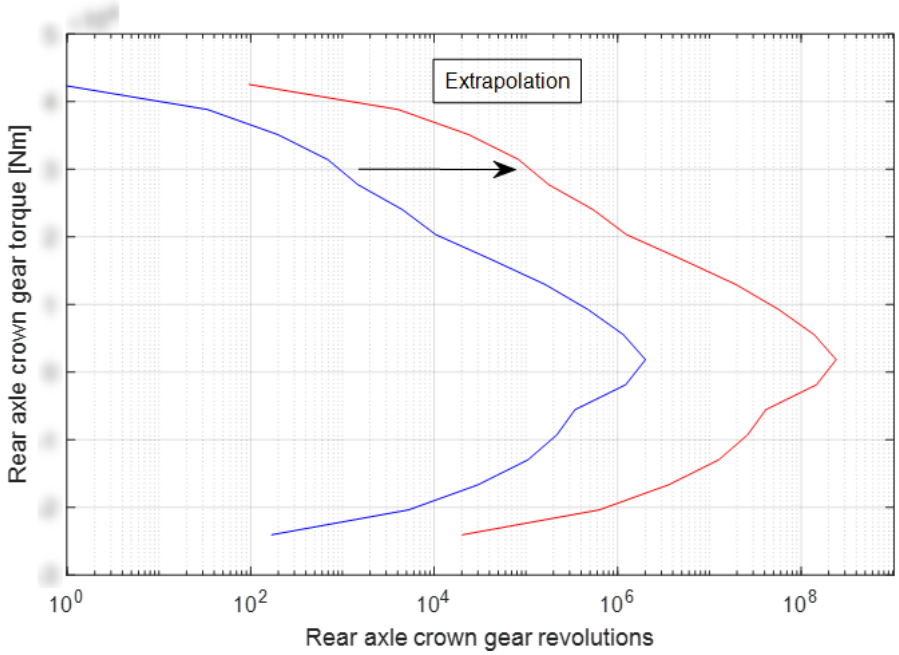

Figure 3: Cumulative exceedance diagram and extrapolation

2.2.3. Durability and fatigue damage

The most widely used model for predicting fatigue damage is the linear model. The linear damage principle considers the Palmgren-Miner failure hypothesis which state that the damage is accumulated in a linear mode and determine that the fatigue failure occurs when the cumulative damage D is equal to unity, according to this equation:

$$D = \sum d_i = \sum \frac{n_i}{N_i} \geq 1$$

The cumulative damage D is defined by the accumulation of the individual damage d_i, defined by the ratio between the number of cycles n_i at a specific stress level σ_i and the number of load cycles to failure N_i, if the component is subjected only to that specific stress level. Considering the fatigue stress vs life curve ($\sigma - N$) with 2 slopes in Figure 4, also called *Wohler's curve*, the main curve [1] has exponent b, while the secondary zone [2] for $N > N_{lim}$ has an exponent higher than b, for example for cylindrical gears $b = 2b - 1$. The relation to determine the number of cycles to failure N_i can be expressed as follows:

$$N_i = N_{lim} \left(\frac{\sigma_{lim}}{\sigma_i}\right)^b$$

where N_{lim} is the number of cycles at the knee point in the fatigue curve, between zone 1 and 2, σ_{lim} is the correspondent stress level and b is the *Wohler exponent*.

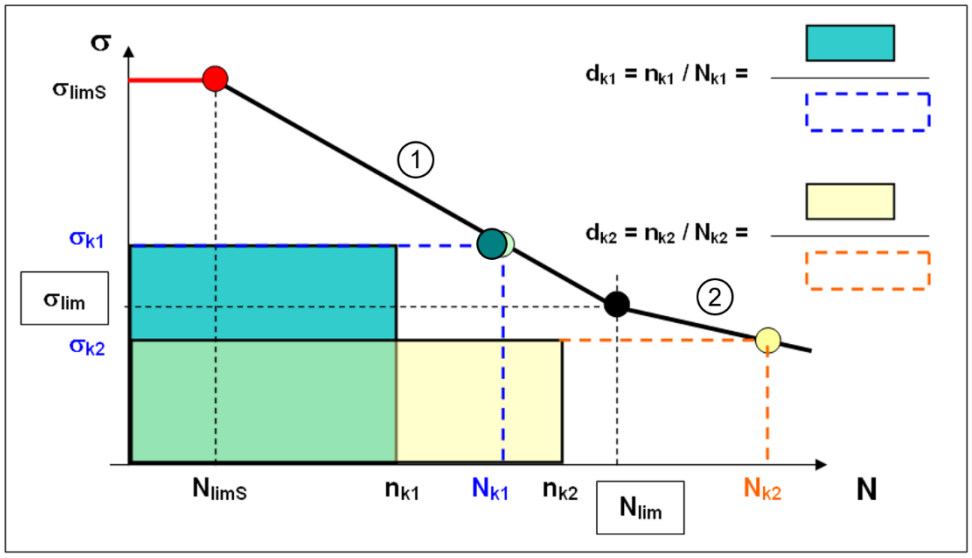

Figure 4: Fatigue S-N curve (Wohler curve) with 2 slopes

It can easily be deduced that, the relative damage is function of the section of the fatigue curve and so the total cumulative damage can be expressed as follow:

$$D = \sum_{k1} d_{k1} + \sum_{k2} d_{k2}$$

considering d_{k1} e d_{k2} the relative damages in the respective zones. It should be noted that the Palmgren-Miner criterion and the consequent life predictions with the Wohler diagram are applicable in areas of the curve far from the yield conditions of the material and low cycle fatigue.

A mechanical component such as a transmission is made up of different parts such as bearings, shafts and gears which are stressed in different ways and therefore are characterized by different fatigue damage modes. For example, gears are subjected to a cyclic bending moment, while bearings suffer fatigue damage due to rolling contact of the rolling elements in the inner and outer rings. Over the years, scientific research and field experience have made it possible to derive formulas capable of estimating the life of these components with great reliability, in particular for bearings, considered among the most sensitive mechanical components to the various operating modes. For each component a different exponent b has been derived for the Wohler equation, which

allows to correlate the stress to the number of cycles to failure. Here in the table below some of the most used in mechanical design.

Wohler exponent *b* *(durability)*	Bearings (ball - roller)	Cylindrical gears	Bevel & Hypoid gears	Notched shaft (pulsating torsion)	Halfshaft (pulsating torsion)
Bending stress					
Contact stress					

Table 1: Wohler exponent b for different components

2.2.4. Damage number and equivalent conditions

To verify the fatigue resistance of a component for its term life defined in the design phase, the Palmgren-Miner model is used to obtain an equivalent damage number correspondent to a reference duty cycle. This allows to compare different duty cycles and therefore to define a test bench cycle which results in fatigue damage of the mechanical components in the same way of the duty cycle. The damage number is defined as:

$$d_i = n_i {C_i}^k$$

referring with the index *i* to the i-th condition of torque – speed.

It's possible to transform the duty cycle in an equivalent mono-block with only one step of load. To do so, it is necessary to compute the *equivalent torque, equivalent speed, equivalent damage* and *total revolutions*, reported as follows:

$$C_{eq} = \left[\frac{\sum(n_i {C_i}^k)}{\sum(n_i)} \right]^{\frac{1}{k}}$$

$$v_{eq} = \left[\frac{\sum(v_i t_i)}{\sum(t_i)} \right]$$

$$D_{eq} = \sum n_i {C_i}^k$$

$$n_{tot} = \sum n_i$$

The exponent *k* is called *torque exponent* and it represents the slope of the *T – N* curve, being *T* the torque level and *N* the number of cycles to failure. Considering the logarithmic relationship between load and term life of the Wohler curve, a small variation in the load amplitude implies a significant variation in the life of the component and this is amplified as the torque exponent increases.

This kind of behaviour is exploited to accelerate fatigue tests, by setting a higher load the failure mode is not affected, but important reductions in the test duration are obtained. Each component stressed under fatigue load is associated with a different torque exponent *p* due to the different fatigue damage method and the different type of metal alloy used for its construction. The typical value of the torque exponent *k* for the different components of the transmission and for the associated fatigue damage method are reported in the following table:

Torque exponent *k* *(equivalent torque)*	Bearings (ball - roller)	Cylindrical gears	Bevel & Hypoid gears	Notched shaft (pulsating torsion)	Halfshaft (pulsating torsion)
Bending stress					
Contact stress					

Table 2: Torque exponent k for different components

Normally, for an estimation of a complete driveline damage, an average value between bearings, notched shaft and gears is considered.

2.2.5. Accelerated fatigue test

When a durability target is given, an accelerated fatigue test on a test bench have to be set up to be equivalent in terms of fatigue damage to the duty cycle.

The method used to accelerate the test is to develop a cycle with one block of load, considering that the total damage must be the same of the equivalent damage of the duty cycle representative of the vehicle life. Once calculated equivalent torque and speed of a generic duty cycle it is possible to evaluate the duration of the accelerated test T_{test} at a chosen level of torque and speed, using the following formula:

$$T_{test} = T\left(\frac{v_{eq}}{v_{test}}\right)\left(\frac{C_{eq}}{C_{test}}\right)^{k}$$

This procedure is done assuming different values of the torque exponent, typically the following are the most used, representative of the components:

for Bearings:	k = --
for Gears:	k = --
for the complete transmission:	k = --

To obtain an accelerated test with a relatively short duration, the acceleration introduced is strong and this consequently causes an increase in the test torque which must remain within the limits of the maximum torque that can be tolerated by the component. Considering the diagram in the following figure, having chosen a test duration T_{test}, by interpolating the two curves respectively, the two test torques are obtained respectively for bearings and gears. As can be seen, in order to have equal damage of bearings and gears, the respective components should be tested with very different torques, since the test torque for the bearings is higher than that of the gears. Assuming to choose one of the two test torque, for example that of the bearings $C_{test,bearing}$, it is found that the correct duration that should be had in order to have the equidamage on gears is less than the T_{test}. From this it can be clearly deduced that by testing the transmission with a duration T_{test} greater than $T_{test,\ right\ for\ gear}$, there is an overstress on the gears. On the contrary, always choosing the test duration equal to T_{test}, but with the test torque equal to $C_{test,gear}$, there would be an understress on the bearings, considering that the test duration to have the bearings equidamage should be $T_{test,\ right\ for\ bearings}$.

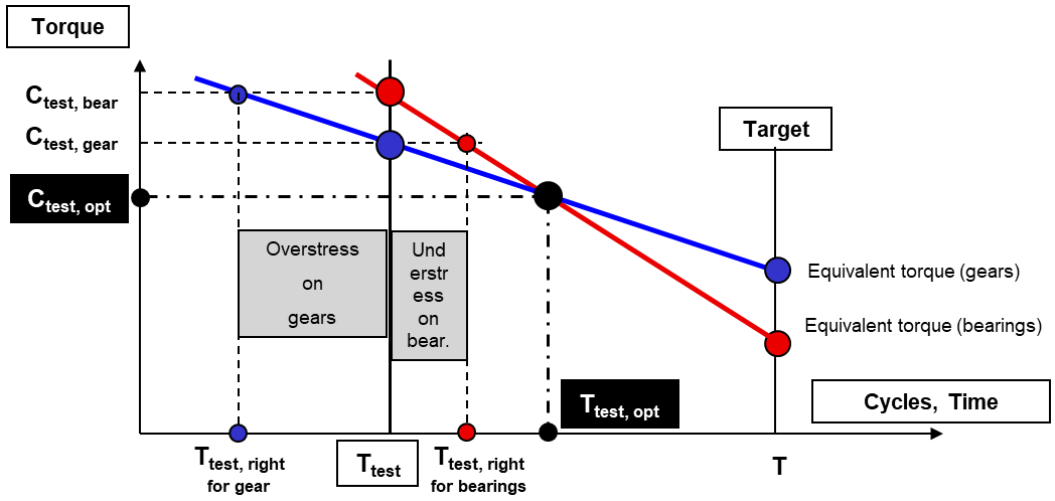

Figure 5: Torque - Time diagram for accelerated test

The goal is to get an accelerated test time that gives simultaneous damage on gears and bearings and, considering that, on the Torque - Time diagram, the damage lines of the different components have different slopes following a different exponent *k*, it is necessary to find the point of intersection between the lines to get the optimal accelerated test torque and duration $C_{test,opt}$ and $T_{test,opt}$ can be calculated with the following formulas:

$$C_{test,opt} = e^{\left[\frac{\log\left(\frac{C_{eq,gears}{}^{m}}{C_{eq,bearing}{}^{n}}\right)}{m-n}\right]}$$

$$T_{test,opt} = T\left(\frac{C_{eq,n}}{C_{test,opt}}\right)^{n}$$

The coefficients *m* and *n* represent the torque exponent *k* for gears and bearings, respectively.

2.3. Test definition

The following section describes the process used to define the bench durability test starting from the analysis of some vehicular missions representative of the road usage profiles during the vehicle life.

In the first part of the section, the data relating to torque and speed of each mission are first analysed to extrapolate the operating map of the electric motors, then the analysis focuses on the clustering of all the other data acquired, relating to the operating temperatures of the various components, in such a way as to have a correlation between the data acquired on the vehicle and the bench test.

2.3.1. Mission profiles

The data was acquired from trucks that covered four different missions, shown in the following table, representative of four typical conditions of usage of the vehicle. The first mission is called "Drayage", representative of a short distance route, typical of a transport of goods carried out with origin and destination in the same urban area. The second mission called "Metro" refers to a road profile typical of a transport in a metropolitan area, on city traffic streets. The "Regional" mission is the one with a highest mileage, typical of a mixed road profile on extra-urban and regional roads. The mission four called "Highway" is instead referred to a motorway route with variable gradients.

Mission	Road Profile	Time [h]	Distance [km]	Time @> 90 km/h [%]	Percentage mileage in average vehicle life [%]
1	Drayage				10
2	Metro				10
3	Regional				20
4	Highway				60

Table 3: Mission profiles representative of the average vehicle life

For each of these missions, the vehicle is instrumented with telemetry sensors, strain gauges and temperature sensors for collecting wheels speed, torque and temperature of the different components. The acquisition system acquires all the data with a sampling rate of 10 Hz and recorded them for all the mission. The torque and speed data referring to the wheels were collected in data files as function of Time.
The following figures show the torque and wheel speed data acquired for each mission.

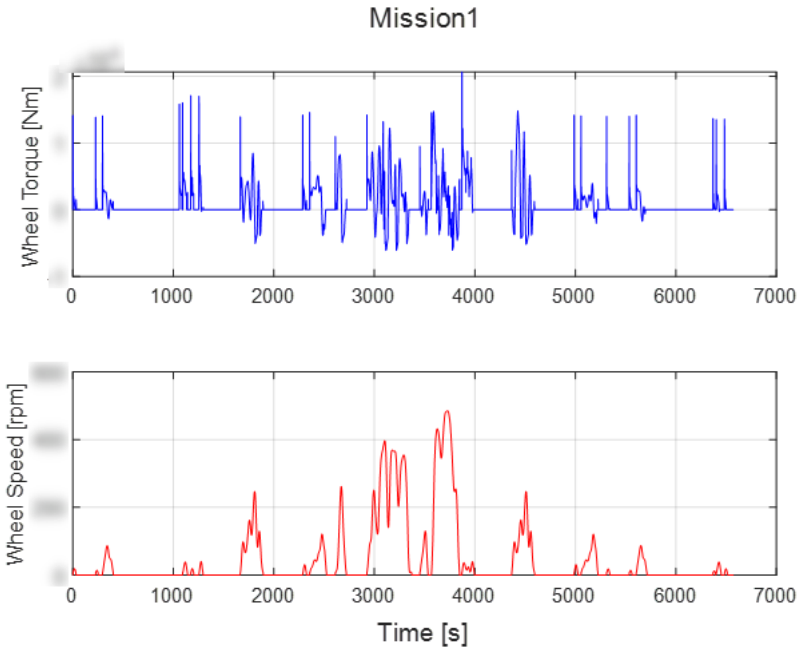

Figure 6: Wheel Torque and Wheel Speed in Mission 1

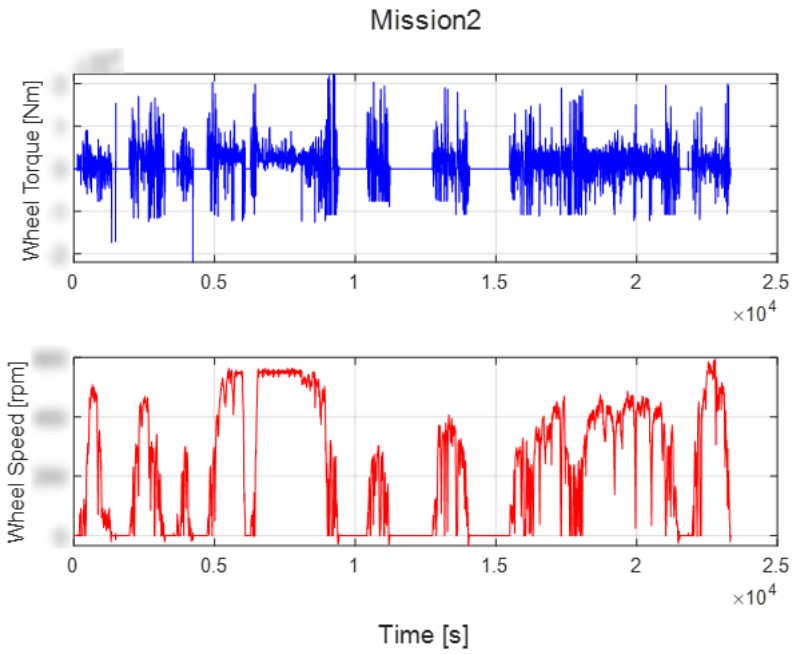

Figure 7: Wheel Torque and Wheel Speed in Mission 2

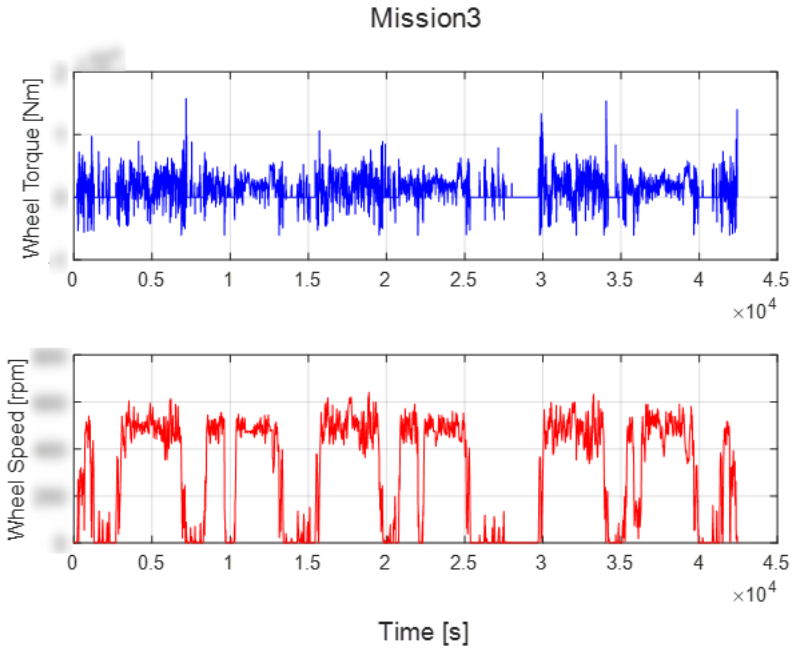

Figure 8: Wheel Torque and Wheel Speed in Mission 3

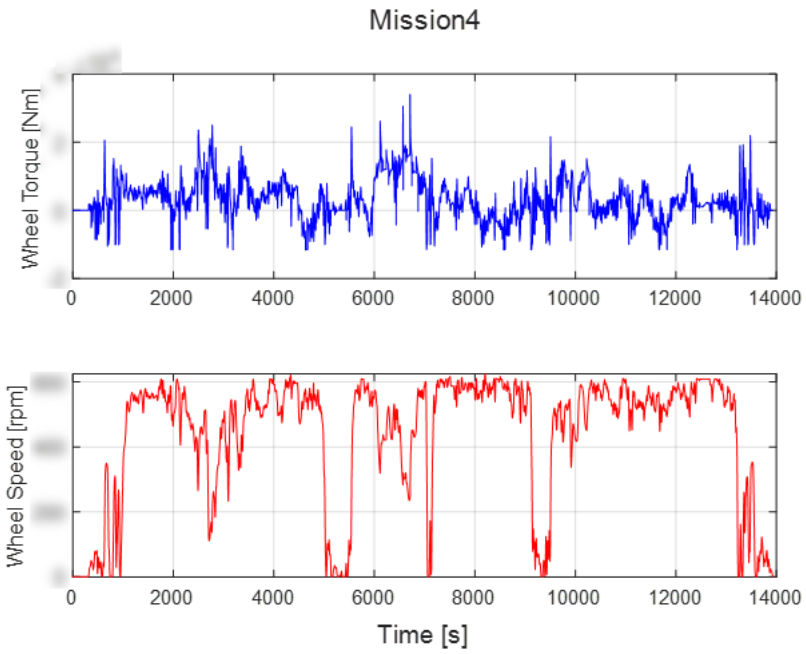

Figure 9: Wheel Torque and Wheel Speed in Mission 4

2.3.2. Missions data elaboration

The first objective is to calculate the input revolutions at each level of torque and speed during all the mission. For this purpose, a code was implemented in *MATLAB®* that allows to extrapolate for each mission a range matrix of Torque – Speed. The revolutions can be organized in a double entry table of Torque – Speed which allows to visualize the range in which the input revolutions accumulate during the mission. Having decided a discretization of the torque range and speed range, to calculate the number of input cycles corresponding to each range of torque and speed, iterative loops were implemented that allows to accumulate the input revolutions in each bin corresponding to the single working condition range. In this way the e-Motor Torque and Speed in each mission can be represented with histograms as a function of the revolutions of the electric motor.

The following figures show the diagrams for each of the missions analysed as a function of the e-Motors cycles as a percentage of the total.

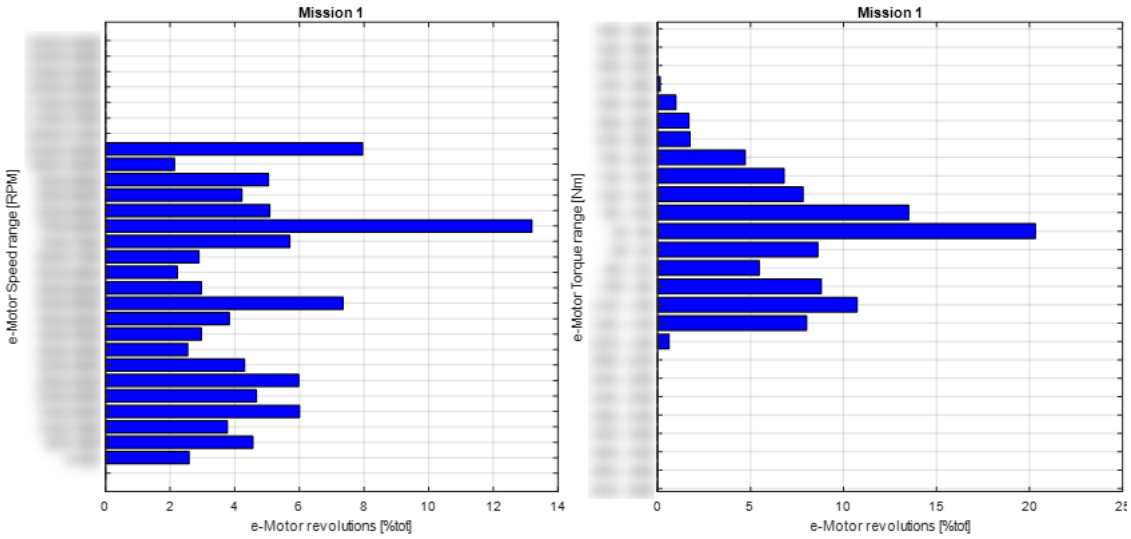

Figure 10: e-Motor Speed and Torque range in Mission 1

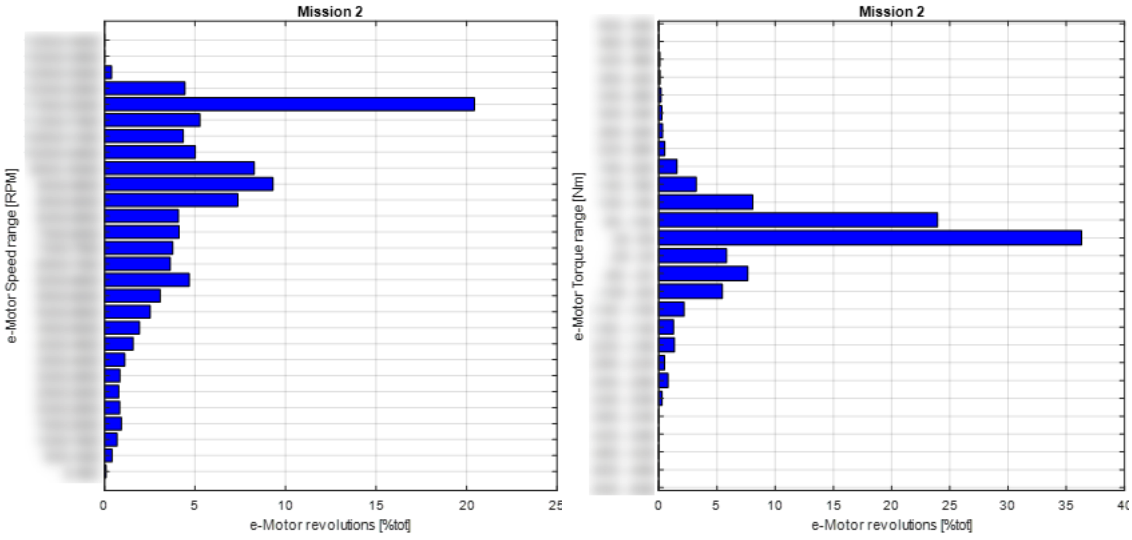

Figure 11: e-Motor Speed and Torque range in Mission 2

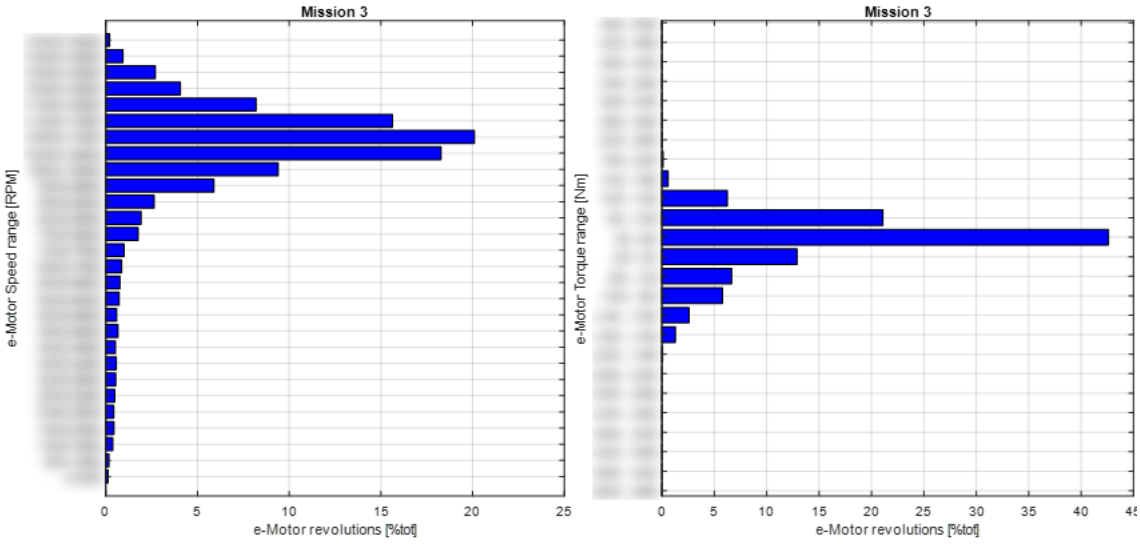

Figure 12: e-Motor Speed and Torque range in Mission 3

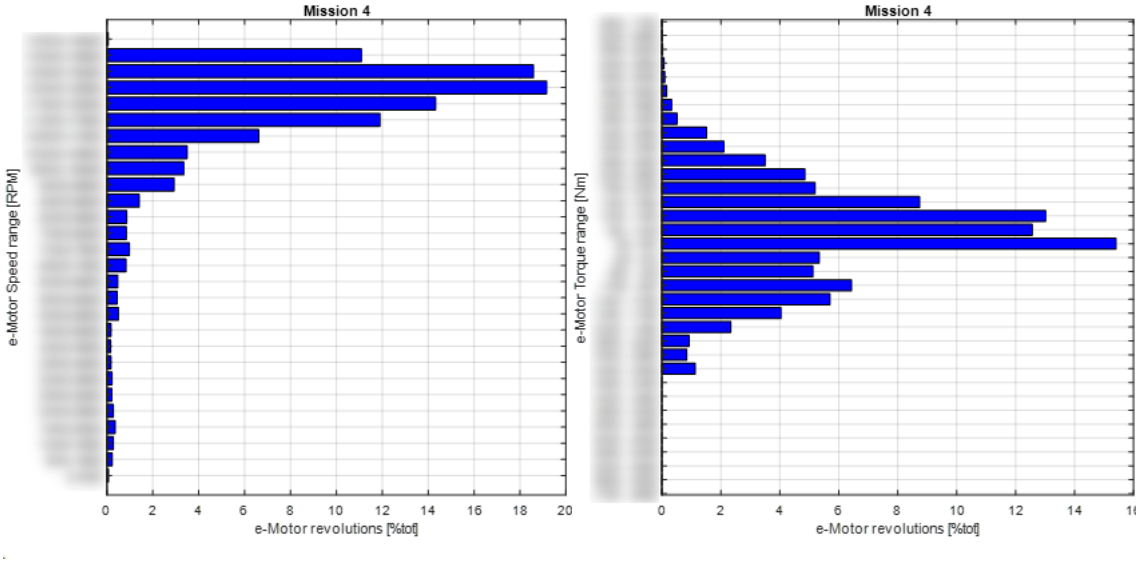

Figure 13: e-Motor Speed and Torque range in Mission 4

The histograms obtained make it possible to clearly identify which speed range and torque range are involved in the various missions and at which levels the most revolutions of the electric motor are accumulated. As can be seen from the Figure 10, Mission 1 has a rather variable and relatively low average speed of the e-Motors, being a mission traveled on urban roads with medium-low loads. The same can be said about the second mission in Figure 11, even if the average speed increases, but the required torque decreases. On the contrary, the speed histogram relating to Mission 3 (Figure 12)

is very different from the previous ones, being a mission traveled on extra-urban roads the average speeds are much higher, reaching even the maximum speed of the electric motor, but the speed range in which the most revolutions are accumulated is at a medium-high level. The load to which the electric motors are subjected is quite low, similar to mission 2. Totally different from all missions is the fourth, traveled on the highway, as can be expected it shows very high speeds close to the maximum, with most of the cycles accumulated at high speed. Unlike the third mission, the latter also seems to be the most demanding in terms of load as the torque of the electric motor is quite high.

Another way to visualize the operating range of the electric motors during a mission is to visualize the map of the electric motor as a function of torque and speed and plot the number of cycles accumulated in each bin of the matrix with level curves. In Figure 14, the e-motor map in mission 4 is shown as an example with a zoom of the area where much more cycles are accumulated, i.e. at high speed.

To allow a comparison between the different missions in terms of damage, it is necessary to refer them all to a common route. By calculating the mileage of the vehicle in the analysed duty cycle from the number of wheel revolutions, it is possible to extrapolate the number of cycles for a normalized distance, multiplying the revolutions by a multiplication factor (*K1*) which is obtained from the ratio between the distance chosen as a reference and the distance traveled in the mission analyzed.

$$K1 = \frac{normalized\ distance\ [km]}{mission\ mileage\ [km]}$$

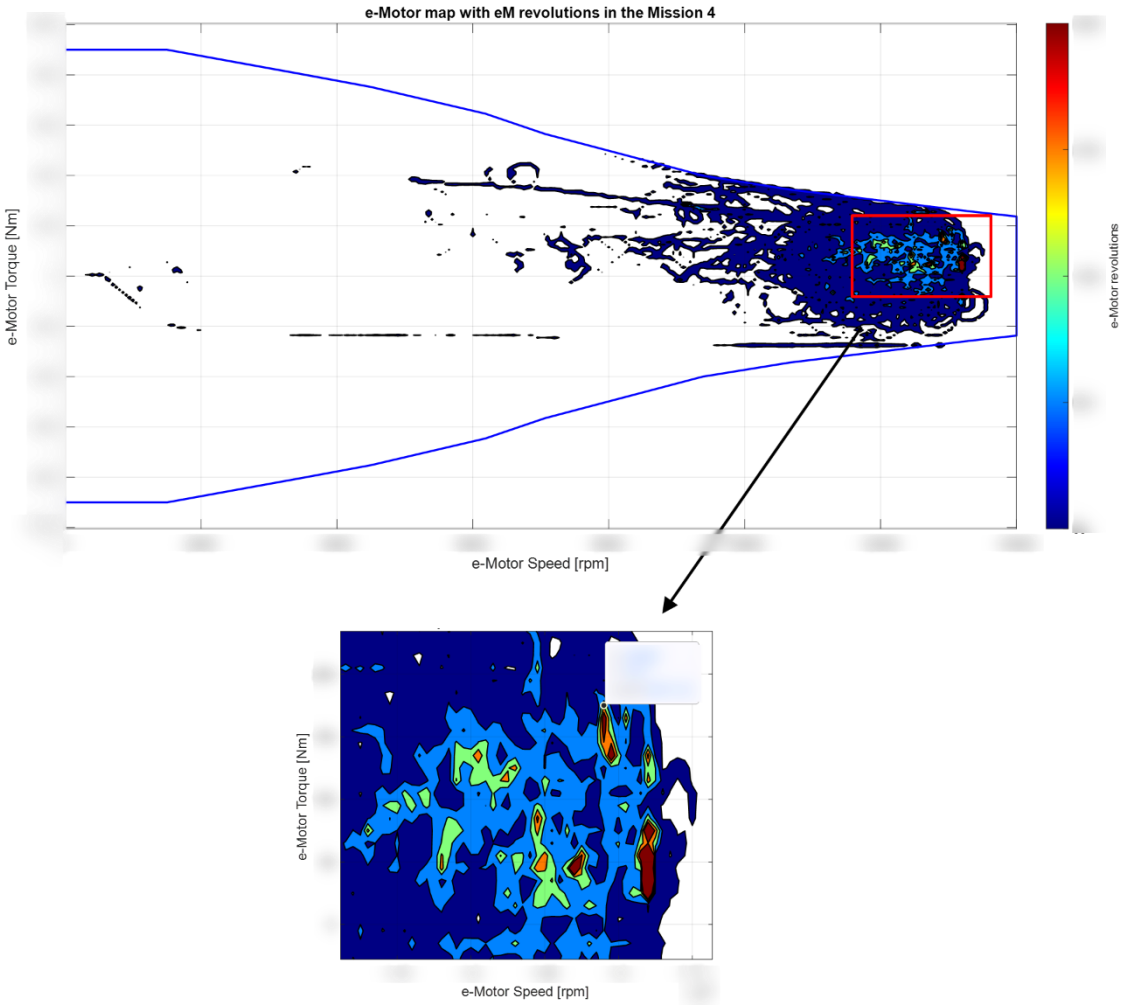

Figure 14: Mission 4: e-Motor Torque-Speed map with eM revolutions

The cumulative load diagrams can be obtained by cumulating the cycles for each torque level starting from the maximum level of torque in decreasing order up to zero torque for the drive condition and then in a specular way for the coast condition starting from the minimum torque up to zero. As previously explained, these diagrams are only a method to display the spectrum of the load acting in a determined duty cycle and for torque equal to zero, the total number of wheel revolutions is read. In this way, it is possible to compare the different vehicular missions and to see at which torque level the most revolutions accumulate. In this analysis, both the revolutions and the torque refer to the wheels of the vehicle, obtained respectively by dividing and multiplying the data relating to the electric motor by the overall gear ratio of the transmission.

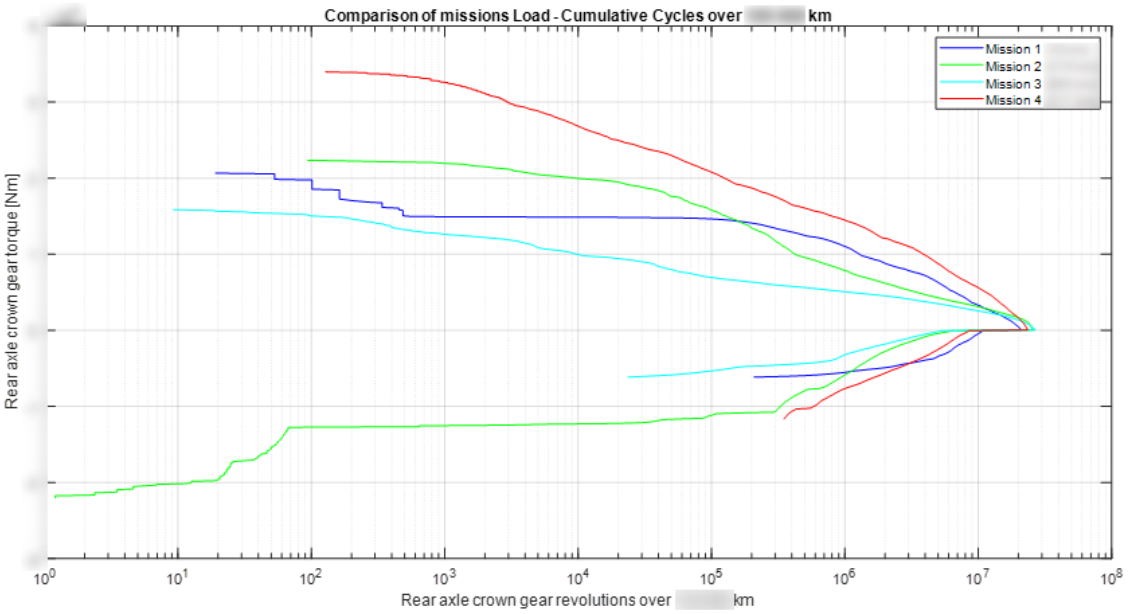

Figure 15: Diagram of load – cumulative cycles for the four missions

As can be easily deduced from the graph in the Figure 15, mission 4 is the most demanding in terms of load above all the missions analysed, as the revolutions are accumulated at higher torque levels than in all the other missions.

2.3.3. Equivalent Duty cycle

To have a numerical reference of the fatigue damage that causes each mission, the equivalent damage is calculated for each one, considering the drive conditions separately from the coast ones. For each block of the torque – speed matrix, the respective damage number is calculated, with the formula previously described. By cumulating the damage calculated for each block, the *equivalent* conditions of damage, torque and speed of the analysed duty-cycle are obtained, for each torque exponent *k* considered. The calculation was carried out considering the torque exponents relating to the S - N curves of bearings, gears and one which is representative of the complete transmission.

Table 4 shows the equivalent conditions calculated for each mission using the formulas described in the previous section with the respective damage numbers, all referring to the same target distance. Mission 4 results to have an equivalent damage of at least one order of magnitude higher than the others and also the equivalent torque for the various exponents *k* are far higher than all the others.

In defining a cycle for an accelerated durability test, it is necessary to take into account the estimated travel percentage of each mission in the real life of an average

vehicle. For this reason, the equivalent damages calculated for each mission must be extended to the maximum target mileage of the vehicle, taking into account the contributions of the individual missions. As shown in Table 3, mission 4, in addition to be the most onerous as we have seen in terms of fatigue damage, is also the one that represents about 60% of the total kilometers travelled by the vehicle during its life, while the others in order are mission 3, which represents 20% and missions 1 and 2 which represent 10% each, being urban cycles rarely travelled by vehicles of this type. The equivalent damage number is then calculated by multiplying the damage number obtained in each mission for the normalized distance by a coefficient (*K2*) that takes into account the vehicle's maximum target mileage and the representative percentage of that mission in the total vehicle mileage. The coefficient *K2* is defined in the following formula:

$$K2 = \frac{target\ mileage\ [km]}{normalized\ distance\ [km]} \cdot PT$$

where *PT* stands for percentage travelled.

Ref. mileage:		km									
MISSION 1	**Equivalent torque**			**Eq. speed**		**Time/cycle**	**K1**	**Tot. Time**	**Damage number**		
	(Nm)	(Nm)	(Nm)	(rpm)	(km/h)	(h)		(h)			
DRIVE											
COAST											
mileage/cycle		km			TOT						
MISSION 2	**Equivalent torque**			**Eq. speed**		**Time/cycle**	**K1**	**Tot. Time**	**Damage number**		
	(Nm)	(Nm)	(Nm)	(rpm)	(km/h)	(h)		(h)			
DRIVE											
COAST											
mileage/cycle		km			TOT						
MISSION 3	**Equivalent torque**			**Eq. speed**		**Time/cycle**	**K1**	**Tot. Time**	**Damage number**		
	(Nm)	(Nm)	(Nm)	(rpm)	(km/h)	(h)		(h)			
DRIVE											
COAST											
mileage/cycle		km			TOT						
MISSION 4	**Equivalent torque**			**Eq. speed**		**Time/cycle**	**K1**	**Tot. Time**	**Damage number**		
	(Nm)	(Nm)	(Nm)	(rpm)	(km/h)	(h)		(h)			
DRIVE											
COAST											
mileage/cycle		km			TOT						

Table 4: Summary table of the equivalent conditions of the four missions

The total equivalent damage number of the duty cycle that will be used as reference for the accelerated test definition is calculated by adding the equivalent damage number for each mission for the drive and coast conditions respectively, while the duty cycle equivalent torque and speed are obtained using the following formulas:

$$C_{eq,duty\ cycle} = \sqrt[k]{\sum \left(PT_i \cdot {C_{eq,i}}^k\right)}$$

$$v_{eq,duty\ cycle} = \sum \left(PT_i \cdot v_{eq,i}\right)$$

The duty cycle conditions obtained are shown in Table 5.

	PT	K2	Equivalent torque			Tot. Time	Equivalent Damage number		
MISSION 1			(Nm)	(Nm)	(Nm)	(h)			
DRIVE	10%								
COAST									
MISSION 2									
DRIVE	10%								
COAST									
MISSION 3									
DRIVE	20%								
COAST									
MISSION 4									
DRIVE	60%								
COAST									

Table 5: Summary table for the Equivalent condition computation for each mission

	Equivalent torque			Eq. speed		Tot. time	Total Equivalent Damage		
DUTY CYCLE	(Nm)	(Nm)	(Nm)	(rpm)	(km/h)	(h)			
DRIVE									
COAST									

Table 6: Summary table for the duty cycle computation

Since the duty cycle conditions are known, it is possible to calculate the duration of an accelerated test with a single step of torque and speed, which has the same damage of the duty-cycle. Once defined the step conditions, the calculation is carried out considering the formula here reported, for all the torque exponents *k*.

$$T_0 = T\left(\frac{v_{eq,duty\ cycle}}{v_0}\right)\left(\frac{C_{eq,duty\ cycle}}{C_0}\right)^k$$

The torque and speed conditions chosen for an accelerated test are the following:

$$C_0 = -\,Nm \qquad n_0 = -\,rpm$$

ACCELERATED TEST	C0	n0	T0		
	(Nm)	(rpm)	(h)	(h)	(h)
			k =	k =	k =
DRIVE					
COAST					

Table 7: Summary table for the accelerated test durations

Significantly reduction in total test duration can be obtained by increasing the test torque and imposing the same damage number as the reference duty cycle. At the same time for such high torque it is necessary to decrease the speed of the electric motors with respect to that obtained in the equivalent conditions of the duty cycle to stay in the range of the e-motor torque curve. Nevertheless, very different accelerated test durations are obtained based on the torque exponent *k* used. These results allow to make a clear assessment of the duration that would require a bench test to verify the fatigue life of the various components of the gearbox. As might be expected based on accelerated test theory, if bearings were to be tested for term life, too many hours of bench testing would be required, resulting in over stress on the gears.

To get an accelerated test that gives simultaneous right damage on gears and bearings, the optimal test torque and test duration $C_{test,opt}$ and $T_{test,opt}$ can be obtained considering the intersection between the two curves on the Torque – Time diagram. The optimal conditions are then calculated with the formulas shown in section 1.8.

OPTIMAL ACCELERATED TEST	C test opt	n0	T test opt
	(Nm)	(rpm)	(h)
DRIVE			
COAST			

Table 8: Summary table for optimal accelerated test conditions

The value of optimal test torque is relatively lower than the previously selected test torque, which obviously implies a much longer test duration. This can hardly be done on a test bench, due to problems related to the costs that an activity of such duration would require.

A solution that is often adopted is to define the accelerated test cycle with the exponent *k* which is an average condition between the torque exponent of bearings and gears, or if possible, use the life calculated with the bearings exponent *k* to be sure of testing completely with the same damage of the duty cycle, while as regards the gears, since they are designed for infinite life, the overstress caused by the test should not cause problems.

2.3.4. Endurance test cycle on bench

The endurance test cycle is defined with two steps of torque in the respective phases of drive and coast with two steps of speed, as showed in Figure 16.

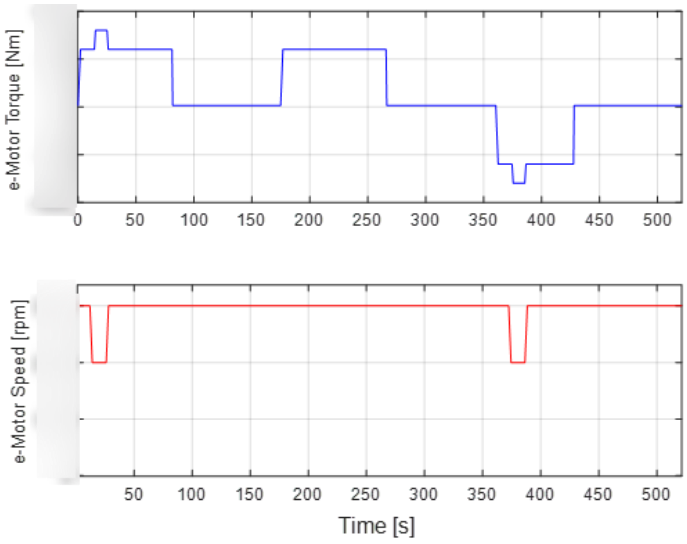

Figure 16: e-Motor Torque and Speed in Endurance test cycle

The test cycle consists of three torque phases, two for driving conditions and one for coasting, while the speed of the e-Motors is set at - rpm for the entire cycle and drops to - rpm min in the two torque steps at - rpm. These phases are interspersed with zero torque phases necessary to cool all the components of the e-Axle, mainly those relating to the electrical power circuit, i.e. stator, rotor and inverter which are particularly thermally affected by the high torque steps. To define the time duration of these phases, the thermal transients were analyzed to maintain the temperature of the components in the typical operating range as in real conditions on the vehicle.

The same damage analysis that is done previously on the missions is repeated on the endurance test cycle to find the number of repetitions that have to be done in order to have an equivalent damage that is the same of the duty cycle. The number of repetitions is iteratively found to reach the damage target obtained in the duty cycle for the exponent k = -. The table below shows the equivalent conditions of torque and speed of the endurance test cycle and the damage number for a single cycle and for N repetitions of it.

ENDURANCE TEST CYCLE	Equivalent torque			Eq. speed		Rep.	Tot. time	Damage number		
	(Nm)	(Nm)	(Nm)	(rpm)	(km/h)		(h)			
DRIVE										
COAST										
					TOT					

DRIVE										
COAST										
					TOT					

Table 9: Summary table for the endurance test cycle equivalent conditions

Figure 20 shows the comparison of the endurance test cycle with all the missions previously analyzed in terms of total wheel torque vs cumulative cycle. The missions are all reported to the common target mileage of the vehicle, while the endurance test shown is referred to the total cycle.

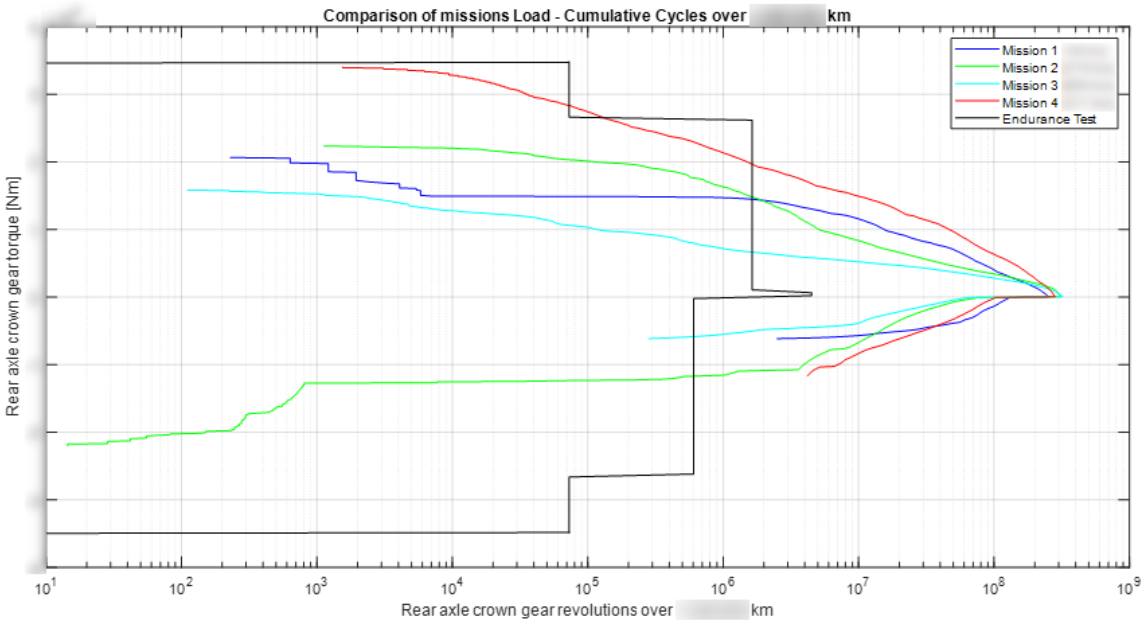

Figure 17: Diagram of load – cumulative cycles for the four missions and endurance test cycle

3. Vibration Monitoring

3.1. Condition Monitoring methods

Vibration monitoring is a specific kind of analysis that can be used to monitor the state of the internal components inside the machine during the test, without the need to stop the test and dismounting the different components to check the status of them.

A machine, during normal operation, emits a certain vibration signature typical of all the components inside it that interacts between each other's, due to the excitation of a forcing term that cause a dynamic response of the system. In the considered case of a gearbox system with two integrated electric motors, the principal excitation sources of the system are the shaft rotation, responsible of the mechanical effects produced by the forces exchanged by meshing gearteeth and the electromagnetic forces generated from the rotating magnetic field of the e-motors that induce specific vibrations that add to the previous one. Since these events in general are periodic, the frequency at which such occur often gives an indication of the source of emission of the characteristic vibration signature. These properties of the system can be successfully exploited with diagnostic techniques based on frequency analysis, to detect which component is the cause of a particular event and then to monitor the health condition of the machine during the operation.

Unfortunately, the vibration signal of the machine measured on the housing, it's the combination of multiple sources covered with noise, so different signal processing techniques must be implemented to extract the useful information from the vibration signal. Moreover, some source of vibrations of the machine are not directly linked to the gearbox shafts rotation, but they are caused by a number of phenomena that often has distinct characteristics, such as the flow of the coolant in pumps, pipes or the splashing of the oil inside the transmission. **(5)**

The advantages of this technique are the relatively easy execution, it does not require particular equipment, since to acquire the vibration signal can be used an acceleration transducer (accelerometer) mounted on the machine cover that does not limit the normal operation, but also the fact that the vibration signal suddenly react to abrupt malfunctioning inside the component, so the response time to unexpected event can be instantaneous.

It is useful to mention also other machine condition monitoring technique that can be used in testing field.

One related to the vibration analysis is based on the acoustic emissions, since when a component manifests a damage, developing cracks or other types of deformations, can change the sound produced during the operation and this can be recorded through microphones or piezoelectric transducer and analyzed to find the noise source. Due to the high sampling frequency required for this analysis, so the large amount of data that have to be collected and to the poor results obtained, vibration analysis outperform the acoustic emission method.

To obtain information about the internal condition of the machine, an analysis can be done on the lubricant that carries information about the presence of contaminants, wear particles and the measurements of viscosity and degradation of the oil. To perform this analysis can be used filters and magnetic plugs (chip detectors) that can retain ferromagnetic particles (called debris) that may separate from the different components. A periodic analysis of the quantity, type, size and shape of these particles can highlight the presence of a damage and discover which kind of component is damaged, since they are constructed with materials with different chemical composition. This is one of the limits of this analysis, since it is able to detect the kind of faulty component and not the specific one, because for example different bearings in the transmission can be made with the same material and the same can be said for the gears. Furthermore, this procedure it's much more difficult to be applied to grease lubricated components and the results of the analysis are not quickly obtainable, since several days may be needed for processing the collected samples.

To evaluate the correct functioning of the machine the performance analysis can be also used. The power adsorbed from the electric motors can be evaluated and compared with the nominal conditions. This analysis can be surely done on the test bench since all the data for the evaluation of the instantaneous mechanical power can be derived from the torque and speed measured from the torquemeters and compared with the adsorbed electrical power, calculating the various efficiencies.

Measuring the temperature with thermocouples of different machine parts that can be reached from outside of the machine, can be useful to detect faulty components since friction can cause a measurable increase in temperature with a consequently significant lack in performance. This analysis it's not able to detect damage at the early stages, because the rise in temperature for example in bearings usually occurs in the final stages of life when rolling elements begin to slide. Thermography analysis can be also done with a thermal imager, a non-contact temperature measurement device which gives the possibility to measure also the temperature of rotating parts, such as shafts and rotors.

Among all these methods, vibration analysis shows the largest amounts of advantages with respect to all the others, since its ability to detect and isolate the faulty

component from the analysis of the vibration signals with different signal processing techniques. To increase the possibility of identifying a fault, vibration monitoring can be done in parallel with other monitoring techniques such as thermography with the continuous acquisition of temperature data of different component for all the duration of the test. **(5)**.

3.2. Continuous vs Intermittent monitoring

Condition monitoring of the machine during the test with vibration analysis can be implemented in two ways, that depends from which kind of information we want to extract from the vibration signal. Since the accelerometers can be mounted on the housing of the machine in a permanent way for all the duration of the test, both the monitoring techniques can be used, but for different purposes.

The continuous or permanent monitoring allows to detect a possible damage inside the machine in a very quick way, given the possibility to react before the occurrence of the catastrophic event and protecting all the other components or expensive equipment that may be involved. This is usually done by monitoring, in a continuous way, some relatively simple parameters such as RMS, Peak to Peak vibration level capable of triggering an alarm if a pre-established threshold is exceeded. The drawback of this analysis is that in general these parameters do not give large advance of detection of the incipient failure in terms of time, it may be some hours or few days in comparison with more advanced techniques that can give this information much earlier. Furthermore, continuous monitoring has only the scope to give a warning of an impeding failure but the not its type, intensity or location. To fulfill this purpose it is possible to analyze the signals in more details, but not continuously.

An intermittent monitoring can be performed as more detailed analysis, carried out in parallel with continuous monitoring with the acquisition of data at pre-established time intervals or in particular conditions during the running of the test. This analysis can give a long-term advance warning of possible faults, with a relatively small data storage, but a more advanced post-processing of the data acquired from the accelerometers is necessary. **(5)**

As it's evident, combining both these techniques can be enhanced the chance to detect a fault, but in the case of carrying out a test on the bench, if priority should be given to one of the two, surely the continuous monitoring of some vibrational parameters and the temperature level of some components, oil or cooling liquid is essential to trigger a pre-set alarm if a certain threshold is exceeded and to stop the machines in automatic way.

3.3. E-Axle vibration signals

The vibration signals of a complex electromechanical system such as an e-Axle, which contains shafts, gears, bearings and e-Motors, is the ensemble of the different source effects that excites the overall structure and, through their transmission paths, they can be measured using a transducer. The main scope in this work is to exploit the characteristics of the signals emitted by the different components to distinguish between the faulty and healthy condition and to recognize which component is damaged. The main issue encountered is concerned with the recovery of the individual effects of each excitation source to the system, caused by the simultaneous operation. This kind of analysis is usually designated as "source separation" and consists in identifying the source of the vibrational signal from the measured global response.

In the e-Axle considered, the main sources of vibrations are the meshing gears inside the gearbox, the rolling elements bearing damages, stator and rotor of electric motors and the overall electric and mechanical noise.

3.3.1. Signals classification

In order to do to understand how the different components affects the machine vibration response, it is necessary to identify the characteristics of each signal emitted by the different components.

A general signal classification can be described as follows **(6)**:

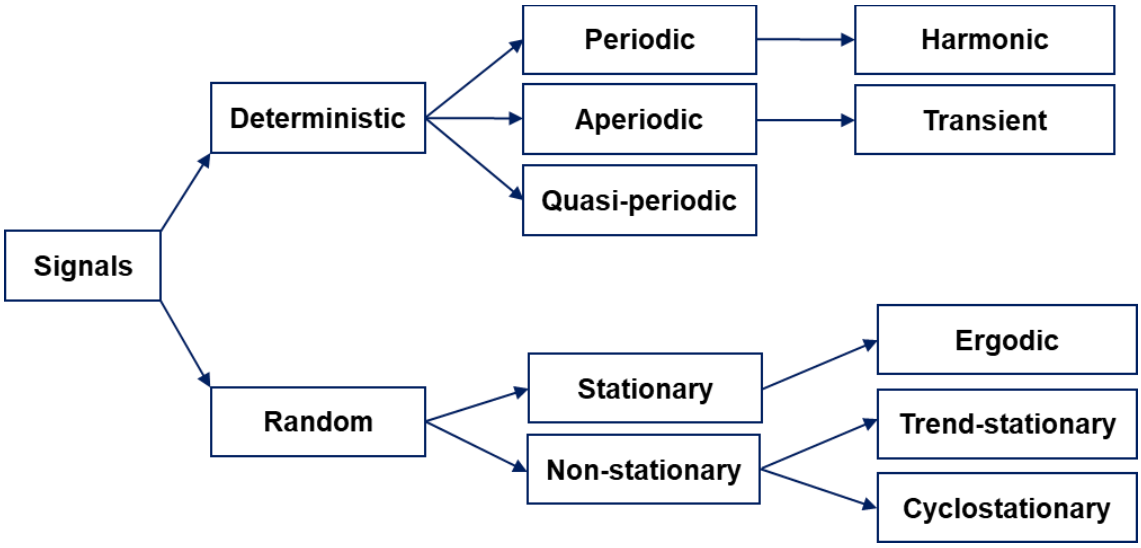

The fundamental division is between *deterministic* and *random* signals, where the first refers to all the signals that can be predicted in the future or the past, once the frequency, amplitude and initial phase are known. Random signals are all those signals that cannot be predicted, but stationary random signal are all those have their statistical properties that do not vary with time. On the contrary, among the non-stationary there are the *ciclostationary*, random signals whose statistical properties varies cyclically with time. While, considering the deterministic dichotomy, the *harmonic* are the most relevant signals in mechanical systems. They are composed exclusively by discrete frequency sinusoids and their frequency spectrum shows only discrete lines at the specific frequencies.

In the literature there are several methods that can be used to separate the two contributions. Some exploit the property of the periodic signal of the gears which can be predicted, implementing some adaptive filters to the signal. One of the most used techniques is Time Synchronous Average (TSA), an effective algorithm capable of extracting the deterministic signal by calculating the average of a series of segments of the signal, each corresponding to a period of shaft rotation.

3.3.2. Gear signals

The spectral analysis of a gearbox shows frequencies attributable to the meshing of the gears. These signals, as known from the literature, are deterministic, in fact since the characteristics relating to a period of rotation of the shaft are known, the gear signal can be predicted for each successive time instant.

Considering a speed reducer, or equivalently, a torque multiplier, it consists of two gears with different diameters and number of teeth, coupled to two shafts that rotate at different speeds. The transmission ratio ($\boldsymbol{\tau}$) between input and output is obtained as follows:

$$\boldsymbol{\tau = \frac{\omega_{OUT}}{\omega_{IN}} = \frac{n_{OUT}}{n_{IN}} = \frac{z_{IN}}{z_{OUT}}}$$

where $\boldsymbol{z_{IN}}$ and $\boldsymbol{z_{OUT}}$ represent the number of teeth of the gears on input and output shafts, $\boldsymbol{\omega}$ and $\boldsymbol{n}$ are the shaft speed in $\boldsymbol{rad/s}$ and in $\boldsymbol{rpm}$.

The typical vibration spectrum induced by this kind of components, it's composed by different characteristic frequencies, that depends by the shaft speed, load and number of teeth. The rotational frequencies are obtained as follow:

$$f_{IN} = \frac{n_{IN}}{60} = \frac{\omega_{IN}}{2\pi}$$

$$f_{OUT} = \frac{n_{OUT}}{60} = \frac{\omega_{OUT}}{2\pi} = \tau f_{IN}$$

The frequency of teeth impact is computed as a product of the number of teeth z and the gear rotational speed f_r in Hz and is referred as gear meshing frequency f_{GMF} or fundamental toothmeshing frequency.

$$f_{GMF} = z f_r$$

The vibration spectra of a gear set are affected by different parameters involved in the meshing teeth, such as tip relief, transmission error, contact ratio, that are chosen at the design stage to optimize and reduce the overall noise. However, during gear operation, the teeth deform due to the applied load and this is reflected on the resulting vibration. Different studies have shown that the variation of the applied load varies the amplitude of the vibrational signal at the toothmeshing frequency and this can be seen as an amplitude modulation effect. From this it follows that to monitor the operating conditions it is necessary to compare different vibrational acquisitions with the same load applied each time, different from zero, for obvious reasons which would otherwise cause chaotic vibrations and gear rattle phenomena, which do not respond to failures in gears. These amplitude modulations of the signal appear in the spectrum as sidebands equally spaced around the harmonics of a central frequency (gearmesh frequency). However, it should be noted that these sidebands are also caused by the modulation of the frequency signal, which is a phenomenon due not only to angular velocity oscillations.

During operation, the gears can undergo various types of damage. The gear teeth are subjected to a pulsating alternating load with a non-zero mean, which causes bending fatigue. In general, the most common defects are related to the deflection of the tooth due to the average torque or to the uniform wear on the flanks of all the teeth. In cases of high torque and therefore high contact pressures on the gear teeth, the breakage of the lubricating oil film can cause the phenomenon of *pitting*. A first indication of wear is usually the increase of the second harmonic of the gear mesh frequency; as the wear spread, this manifests itself with an increase of all the harmonics of the toothmeshing frequency. The spacing between the harmonics and between the sidebands and the gear mesh frequency corresponds to the rotational frequency of the gear that caused them, so it is relatively easy to trace the spectrum back to the cause.

3.3.3. Rolling element bearing signals

Rolling bearings are among the most common mechanical parts in rotating machines and their correct functioning is essential. However, they are often the cause of 45-55% of machine failures. **(7)** They allow relative rotary motion between two components and consist of an outer ring, an inner ring and a series of roller elements (balls or rollers) that slide between the two races. Bearing defects can be of various types, the first distinction to be made is between localized and distributed defects. The former is usually the first stage of progress which over time spreads to an area of the surface. When a localized defect occurs on one of the two races, the rotating element passing over it excites the high resonant frequencies of the structure producing a burst that can be detected by a transducer, such as an accelerometer. Considering the kinematics of a rolling bearing, these shocks produce a modulation of the impacts which depends on the load applied on the bearing and on the speed at which the fault passes from the area in which it is applied. Furthermore, when the defect is on a rolling element or on the inner race, the amplitude of the signal varies according to the distance from the transducer; this produces an amplitude modulation of the signal as can be seen in Figure 18.

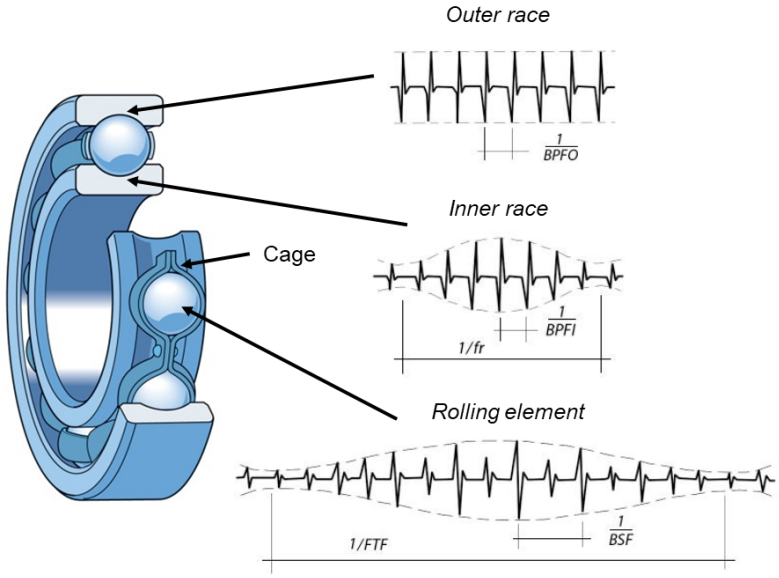

Figure 18: Typical signals from local faults in rolling elements bearings

It is possible to obtain the characteristic frequencies of these impacts for an ideal bearing, as shown below.

- Defect on the outer race:
  BPFO (Ball-Pass Frequency Outer) is the frequency of passage of the rolling elements with respect to a defect on the outer race:

$$BPFO = \frac{nf_r}{2}\left\{1 - \frac{d}{D}\cos \emptyset\right\}$$

- Defect on the inner race:
  BPFI (Ball-Pass Frequency Inner) is the frequency of passage of the rolling elements with respect to a defect on the inner race:

$$BPFI = \frac{nf_r}{2}\left\{1 + \frac{d}{D}\cos \emptyset\right\}$$

- Defect on the cage:
  FTF (Fundamental Train Frequency) is the cage rotation frequency:

$$FTF = \frac{f_r}{2}\left\{1 - \frac{d}{D}\cos \emptyset\right\}$$

- Defects on the rolling elements:
  BSF (Ball-Spin Frequency) is the frequency of passage of a defect present on a rolling element on each of the two raceways, internal and external respectively. Equivalently, it corresponds to the number of revolutions that a rolling element completes at each rotation of the shaft.

$$BSF = f_r \frac{D}{2d}\left\{1 - \left(\frac{d}{D}\cos \emptyset\right)^2\right\}$$

where f_r is the shaft speed, n is the number of rolling elements and $\emptyset$ is the angle of load from the radial plane. D and d are the respective outer and inner ring diameters.
Each of the previous frequencies, if identified on the frequency spectrum with the correspondent higher order harmonics, could indicate a defect present on one of the elements of the rolling bearing.
Those are frequencies calculated for an ideal bearing; in real applications, it is very often observed a deviation of these values from those detected on the spectrum in the order of 1-2%, both due to the tolerances of the system, but also due to the random slippage of the rolling elements due to the different diameter of the rings. For these reasons, the vibrational signature of a bearing is not a periodic signal, but a cyclostationary one.

Usually, these signals are very weak compared to the background noise, so the characteristic frequencies can rarely be identified directly on the spectrum of an accelerometric signal acquired on a gearbox. Therefore, it is necessary to apply specific signal processing techniques to the signal, capable of separating the vibrational contributions of the different components and isolating only the one coming from a damaged bearing. Some algorithms will be shown afterwards, selected from those in the literature, subsequently applied to the vibration signals acquired on the e-Axle during the endurance test.

Bearing faults models

Bearing defects can be of various types, however the most frequent are caused by pitting and spalling phenomena. Pitting is a type of corrosion that appears as small holes on the metal surface generally from contact pressures that are too high or from a localized corrosive attack. At these points the corrosion can penetrate the metal deeply. Conversely, spalling is caused by contact fatigue stress problems due to the rolling of rolling elements on surfaces. This manifests itself in the detachment of metal fragments from the rings and rolling elements.

a) Pitting

b) Spalling

Figure 19: a) Pitting on a bearing outer race, b) Spalling on a bearing inner race

The best way to study the effect of these damages on the generated vibrational signal is to distinguish between localized faults (for example caused by pitting phenomena) and extended faults (for example caused by spalling phenomena).

Generally, in the early stages of development of a fault, it is small and localized on the outer or inner races and generates shocks whenever a rolling element passes over it, which excites the high resonance frequencies of the entire structure between the bearing and the transducer.

The kinematic frequencies reported above are theoretical values, assuming no slip. In reality, there is always some slip because the contact angle ϕ varies during operation as a function of the local ratio of axial to radial load. In this way, each rolling element has a different rolling diameter, therefore it tries to rotate at a different speed, but the cage limits this deviation from the mean position, thus causing random slips which result in a deviation of the bearing frequencies in the order by 1-2%, both from the calculated frequencies and as a random variation from the mean value. (8) These random shifts are the reason why these frequencies cannot be detected in the raw spectrum of the signal, therefore other specific techniques are needed to identify them.

For faults located in the bearings, the model which has proved to be more correct over the years is that of considering the signal generated by them as pseudo-cyclostationary. This model allows to represent the signal period generated by consecutive impacts as a random variable, defined as:

$$\Delta T_i = T_{i+1} - T_i$$

In this way, the uncertainty of occurrence is increasing with the time of prediction into the future, because the system has no memory (8).

As the defect spreads to various points on the surface and becomes extended, every time the element passes over it, there will always be an impact, but as the cracks are large and smooth, they will be of low intensity and therefore difficult to detect. In these cases, it is necessary to investigate the modulation phenomena caused by these on the other components, such as the gears. The vibrational signal induced in the gears undergoes a modulation due to the passage of the extended fault from the loaded area of the bearing.

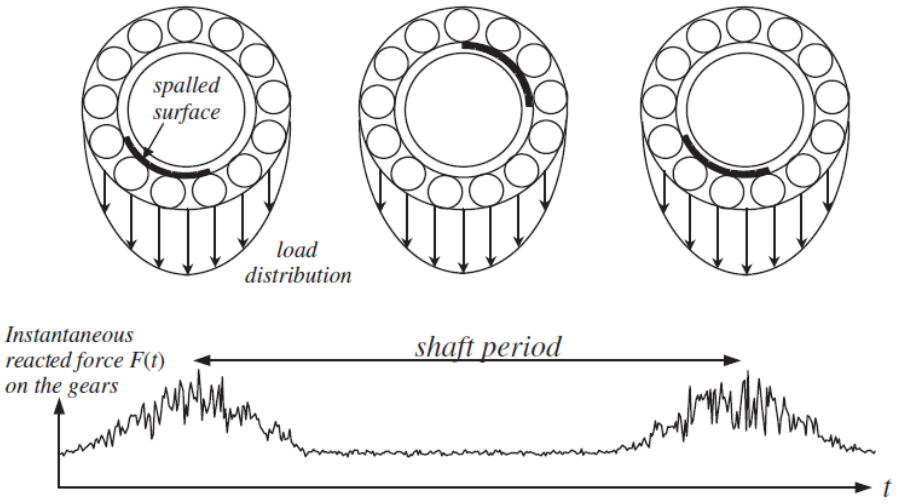

Figure 20: Typical modulation signal from the effect of an extended inner race fault on a gear signal (8)

3.3.4. Electrical machines signals

The vibroacoustic emission of electric machines such as motors and generators is mainly caused by the electromagnetic forces exchanged between the stator and the rotor. The electromagnetic forces can be divided into tangential and radial, of which only the former is responsible for the generation of torque, while the latter generate exclusively a vibrational content which depends on the characteristic parameters of the machine such as the number of poles, the type of electric motor, the shape and frequency of the current. (9) Considering AC electric motors, being the most used in vehicle traction, these generate a rotating magnetic field in the stator which depends on the number of pole pairs of the machine. A first distinction can be made between synchronous electric motors, where the rotor rotates at the synchronous speed of the magnetic field, and asynchronous electric motors or induction motors, in which there is a slip speed between the speed of the magnetic field and that of the rotor, which rotates more slowly.

In the case of the e-Axle analyzed, SMPM (Surface Mounted Permanent Magnet) electric motors are present, which, belonging to the category of synchronous electric machines that have the rotor that is "locked" on the rotating field. In these machines, the characteristic frequencies of the electromagnetic field are obtained by applying the following formulas, reported in (9) :

Stator electric harmonics	$f_1 = 2pnf_r$
Rotor electric harmonics	$f_2 = 2pn(1 \pm 2k)f_r$

with $k = 0, 1, 2, 3 \ldots$, $n = 6k \pm 1$ and where p is the number of pairs of poles and f_r the rotational frequency of the rotor (Hz); Since these components are multiples of the rotation speed, the main difficulty lies in isolating the electrical vibrational component from the mechanical one.

For example, the second harmonic of rotation on the spectrum, could correspond both to a mechanical misalignment of the shaft and to the electric frequency of the stator/rotor field. One way to distinguish the two effects is to disconnect the power supply while in motion and observe the real-time change in the frequency spectrum. The electrical components disappear quickly, while the mechanical ones vary more slowly, being linked to the rotation speed and therefore to the deceleration time due to internal friction and inertia. (5)

3.4. Signal processing

3.4.1. Time domain techniques

The time domain analysis is based on the intrinsic characteristics of the vibrational signal waveform. As can be easily understood, by monitoring the maximum vibrational level of the signal, information on a developed fault of the system can be obtained. However, very often this is not enough to locate the failure before it becomes catastrophic, causing the entire component to fail.

To monitor the progress of the test and the "state of health" of the component under test, it is necessary to post-process the vibrational data acquired by the accelerometers, calculating some "features" which may be indicators of possible damage **(6)**. However, this can be considered a general indication, which does not give information on which component is causing that anomaly. Considering a discrete raw signal $\boldsymbol{x(t)}$, below are some commonly used indicators and their definition **(10)**.

- Mean: it is the arithmetic average of a set of *N* values, defined as:

$$\bar{\boldsymbol{x}} = \frac{\boldsymbol{1}}{\boldsymbol{N}} \sum_{\boldsymbol{i=1}}^{\boldsymbol{N}} \boldsymbol{x_i}$$

- Root Mean Square (RMS): it is defined as the square root of the mean square of a set of signal values. The RMS is also known as the normalized second statistical moment of the signal, i.e. the standard deviation. It is the most used feature for measuring the overall vibration level of a signal, but it increases only at the final stages of failure.

$$x_{RMS} = \sqrt{\frac{1}{N}\sum_{i=1}^{N} x_i^2}$$

- Shape factor (SF): it is the RMS value divided by the mean of the absolute value. It is dependent only by the signal shape while being independent of the signal amplitude.

$$x_{SF} = \frac{x_{RMS}}{\frac{1}{N}\sum_{i=1}^{N}|x_i|}$$

In the early stages, a bearing defect can be detected by the vibration pulses it generates. For this reason, the parameters most used in continuous monitoring are the measurements of signal impulsivity in the time domain and are linked to the measurement of signal peaks.

- Peak value (p): maximum absolute value of the signal.

$$x_p = \max|x_i|$$

- Impulse factor (IF): it compares the amplitude of a peak to the mean level of the signal.

$$x_{IF} = \frac{x_p}{\frac{1}{N}\sum_{i=1}^{N}|x_i|}$$

- Crest factor (CF): it is defined as the ratio between the peak value and the RMS. The crest factor can indicate the presence of a fault before it occurs, as they first manifest themselves in changes in the peak of a signal before the RMS value.

$$x_{CF} = \frac{x_p}{\sqrt{\frac{1}{N}\sum_{i=1}^{N} x_i^2}}$$

To detect defects in rolling bearings, a probabilistic approach is often proposed in the literature, with reference to the probability density function. Instead of studying probability density curves, important insights can be gained by examining the moments of the statistical distributions of the data. Without going into too much detail on the topic, which would go beyond the scope of the thesis, some statistical parameters that can be used as indicators of possible damage are presented below.

- Skewness (skew): it is the third centered statistical moment of a signal and indicates the asymmetry of a signal distribution. It is null for a symmetric distribution, while it increases to positive or negative values when it becomes asymmetric. It can be used for condition monitoring since faults can impact distribution symmetry and therefore increase the level of this indicator.

$$x_{skew} = \frac{\frac{1}{N}\sum_{i=1}^{N}(x_i - \bar{x})^3}{\left[\frac{1}{N}\sum_{i=1}^{N}(x_i - \bar{x})^2\right]^{\frac{3}{2}}}$$

- Kurtosis (kurt): it is the fourth statistical moment of a signal and indicates the length of the tails of a signal distribution. By calculating the kurtosis of the acquired signal, we have an evaluation of its impulsivity. The value of kurtosis is 3 for a normal distribution, i.e. when no impulsive signals are present in a signal, while it increases when the area of the tail of the distribution is greater than the normal and decreases when the area of the tail is reduced. The development of defects can increase the number of outliers and thus can increase the value of the indicator of kurtosis.

$$x_{kurt} = \frac{\frac{1}{N}\sum_{i=1}^{N}(x_i - \bar{x})^4}{\left[\frac{1}{N}\sum_{i=1}^{N}(x_i - \bar{x})^2\right]^{2}}$$

3.4.2. Frequency and Time-Frequency domain techniques

Frequency domain methods are between the most used in the field of signal processing for vibration monitoring. The most known tool is the Fast Fourier Transform (FFT), an optimized algorithm for calculating the discrete Fourier transform (DFT). It is based on Fourier theory has every periodic function *f(t)* of period *T* can be expressed as the sum of sines and cosines, with relative amplitude coefficients, the so-called Fourier series. It can be interpreted as a change of point of view of the signal, from one based on the time domain to one based on the frequency domain. The advantage of this technique is that analyzing the frequency spectrum, certain frequency components of interest can be identified and isolated. This is undoubtedly an advantage above all for the detection of the characteristic frequencies of the defect in the bearings. The problem is that a bearing defect can rarely be seen directly on the frequency spectrum due to the masking of other strong vibrations. Therefore, other techniques based on Fourier analysis will be subsequently treated to achieve the prefixed aim.

A limitation of frequency signal analysis is the impossibility of analyzing non-stationary signals such as those coming from rotating machines. For this reason, a Time-Frequency analysis can be used. This is the case of the so-called Short-Time Fourier Transform (STFT), which applies the Fourier analysis only to a given mobile signal time window at a time. The STFT represents the signal both as a function of the instant of time and of the frequency in a 2D colormap called *spectogram* or in a 3D diagram called *Waterfall* diagram and is therefore able to provide a measurement of the sinusoidal frequency and the phase content of a signal in function weather. The main disadvantage of STFT is that it provides an indication of when and how often a given event occurs but with a precision limited by the width of the window used. Once a size for the time window has been chosen, it remains the same for each frequency analyzed. The time resolution is given by the width of the window in time *dt*, while the resolution is inversely proportional to this frequency (*1/dt*). Therefore, this limitation makes it suitable to analyze only non-stationary signals that have a slow change in their dynamics.

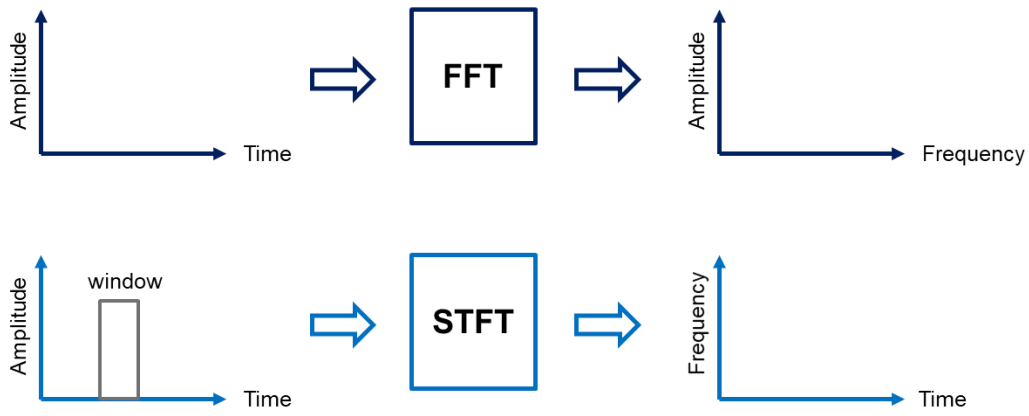

Figure 21: Fast Fourier Transform and Short Time Fourier Trasform

3.5. Bearing diagnostic techniques

3.5.1. Envelope Analysis

The Envelope Analysis (EA) of the accelerometric signal is the reference method for bearing diagnostics. As we have seen, localized defects in bearings cause repetitive shocks that excite the high frequencies of the structure around them. This periodic

excitation causes an amplitude modulation of the high-frequency noise, which turns out to be the carrier signal of the diagnostic information. **(8)** To identify the characteristic frequency of the damaged bearing, it is necessary to demodulate the signal, i.e. obtain the modulating frequency of the signal. The analysis of the envelope of the signal and the visualization on the frequency spectrum allows to identify the characteristic frequencies of the defect. The main problem is that these spectral lines are usually very weak compared to the background noise due to other sources of machine vibrations (gear meshings, rotations of shafts, electrical signals...) and therefore difficult to detect from the analysis of the raw signal. Therefore, to increase the chances of detection, one of the techniques is to apply a band-pass filter to the signal at the resonant frequency of the bearing before demodulation. However, this frequency is often unknown and various techniques are used to identify the correct band, including Spectral Kurtosis.

3.5.2. Spectral Kurtosis and Kurtogram

Spectral Kurtosis (SK) is a statistical parameter that measures the kurtosis value of the signal as the frequency varies, i.e. it is able to provide information on which frequency zone the signal has the maximum impulsivity. The algorithm is based on the STFT and in the same way the SK is obtained by slinding a window over a time interval. The problem of STFT is that it is unable to provide accurate information in frequency and time at the same time, therefore to overcome this issue, J. Antoni developed the Fast Kurtogram. This algorithm computes the SK for different frequency bands, following a 1/3 binary three division of the plane $[\boldsymbol{f}, \Delta\boldsymbol{f}]$. To obtain this division, a FIR filter-bank is applied to the signal and the SK is calculated for each frequency band of the signal. In the present thesis, the Kurtogram will be calculated in *MATLAB®* using the *Fast_Kurtogram.m* function developed by J. Antoni **(11)**.

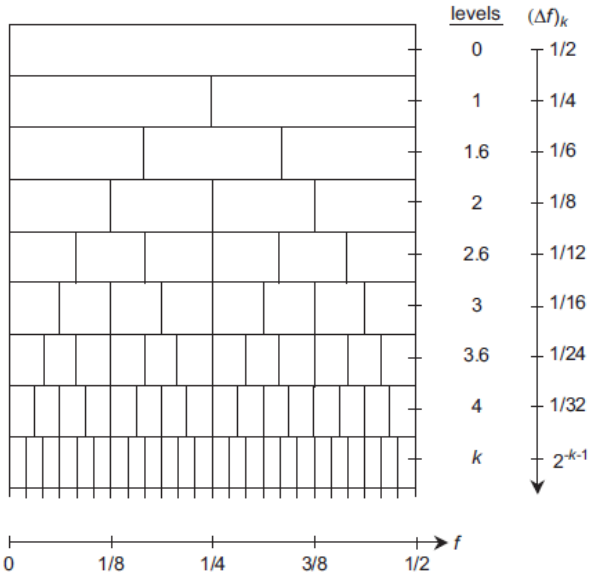

Figure 22: 1/3 binary tree division for the Fast Kurtogram

3.5.3. Cyclostationarity and Spectral Correlation

Most of the signals generated by rotating machines are of the cyclostationary type. It is a property of those signals which, although not periodic, are produced by a hidden periodic mechanism, as they vary cyclically over time. A cyclostationary signal of order n is a random signal showing statistical characteristics of order n of periodic type.

The study of cycle stationarity is fundamental in the diagnostics of rotating machines, in particular for bearings and gears, for various reasons. The first, the occurrence of a fault in a rotating component such as a bearing generates pulses of a cyclic nature, which have all the characteristics of a cyclostationary type signal. Second, because it allows to identify and locate the fault considering the kinematics of the rotating parts. And finally, it makes it possible to distinguish the different types of signals generated by the different sources of the machine, isolating only the contribution of interest for the analysis. In this regard it is necessary to make a distinction between the different orders of cyclostationary, in particular between a cyclostationary signal of the first order and one of the second, but first it is necessary to distinguish between a deterministic and a random signal.

According to Wold's theorem, any signal $\boldsymbol{x(t)}$ can be decomposed as:

$$\boldsymbol{x(t)} = \boldsymbol{\mathcal{P}\{x(t)\}} + \boldsymbol{\mathcal{R}\{x(t)\}}$$

where the predicted value $\boldsymbol{\mathcal{P}\{x(t)\}}$ represents all the periodic or deterministic components of a signal, while the residual part $\boldsymbol{\mathcal{R}\{x(t)\}}$ embodies all the random components present in the signal. The difference between the two is that the random

component, as opposed to the deterministic one, can never be predicted over time. To extract the periodic components of a signal it is sufficient to calculate the average value, which in the case of a stationary signal is always a constant value, while in the case of a cyclostationary signal it is itself a signal with a cyclic pattern **(12)**. This decomposition allows to distinguish between first order cyclostationary, represented by the periodic component, and second order cyclostationary, represented by the residual term.

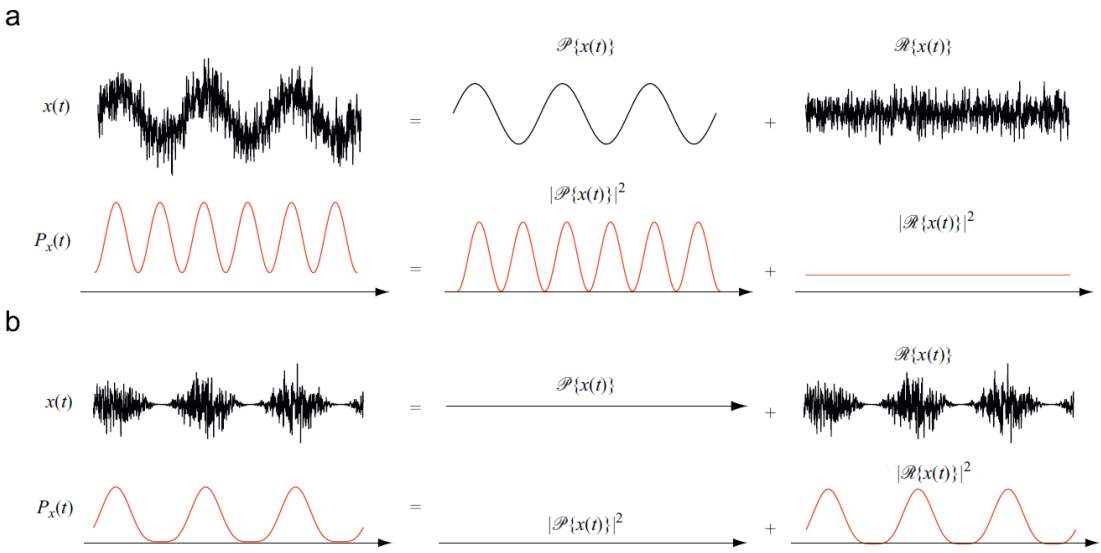

Figure 23: Decomposition of a vibration signal into their deterministic and random parts and their mean instantaneous powers for a first order cyclostationary signal (a) and for a second order cyclostationary signal (b) [image courtesy of (12)]

This concept is better explained by Figure 23, which shows the decomposition of a signal into the corresponding deterministic and random parts, paralleled with their mean instantaneous powers. Figure 23 (a) shows a first order cyclostationary signal that is a periodic signal immersed in background noise. By applying the average value to the signal $\boldsymbol{x(t)}$ it is possible to obtain the separation of the periodic and random contributions. From the parallelism with the instantaneous power $\boldsymbol{P_x(t)}$ it can be seen that the periodic term contributes with a periodic trend of the instantaneous power while the residual with a constant value. On the contrary, Figure 23 (b) shows a second order cyclostationary signal consisting of a white noise signal amplitude-modulated by a periodic signal. By extracting the periodic and random contributions of the noise, the power of the periodic signal is a constant value, while the residual term contributes to the instantaneous power of the signal $\boldsymbol{P_x(t)}$ with a periodic trend.

This approach is significant for distinguishing vibrational phenomena of different nature, as in the case of vibrational signals acquired on gearboxes. In fact, these usually include a deterministic part due to the gear mesh and a random part relating to other

phenomena such as vibrations due to fluid flow, due to friction and also those coming from a defective bearing, according to the bearing model which considers random slips for the rolling elements.

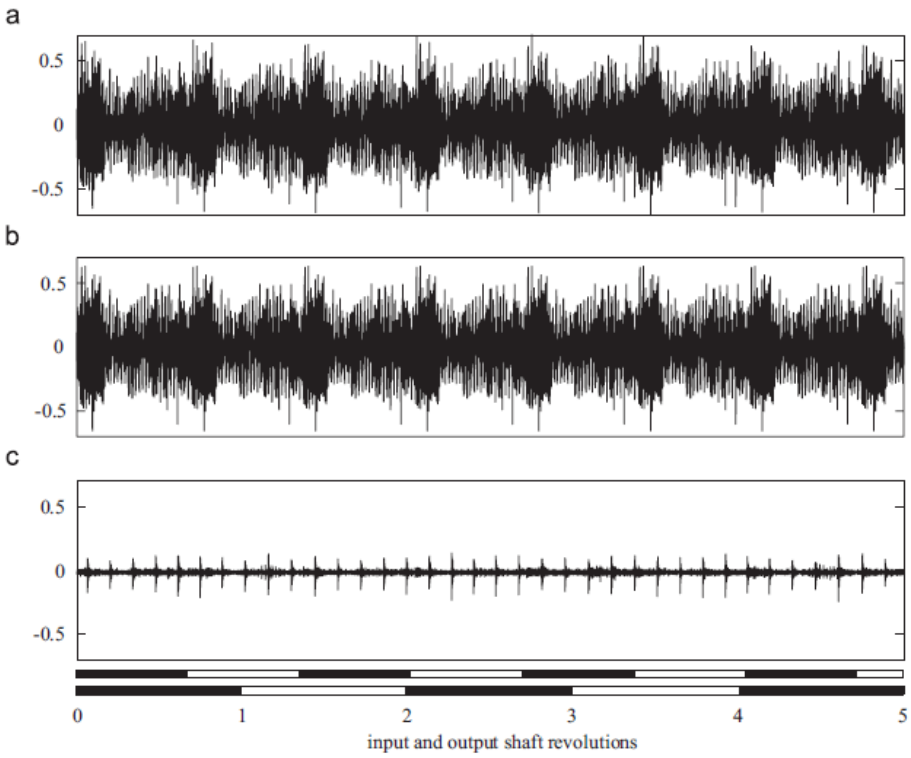

Figure 24: Decomposition of a gearbox vibration signal (a) into its deterministic (gears contribution) (b) and random parts (bearing contribution) (c) [image courtesy of (12)]

As can be seen in Figure 24, the vibration signal of a gearbox is decomposed into the corresponding deterministic and random parts. The first contains the contribution caused by all physical phenomena characterized by a cyclic periodicity, such as shaft unbalancing, eccentricity, misalignment, gear mesh. While the residual term, contains a series of shocks due to a defect located on the outer race of a rolling element bearing. Isolating the different contributions is essential to investigate the different causes of the phenomena. However, these signals are statistically very different, therefore they require to be analyzed with different tools. For the periodic, first order cyclostationary part, undoubtedly the most valid and most used method is the classic Fourier analysis, while different tools are needed to represent a cyclostationary signal of the second order.

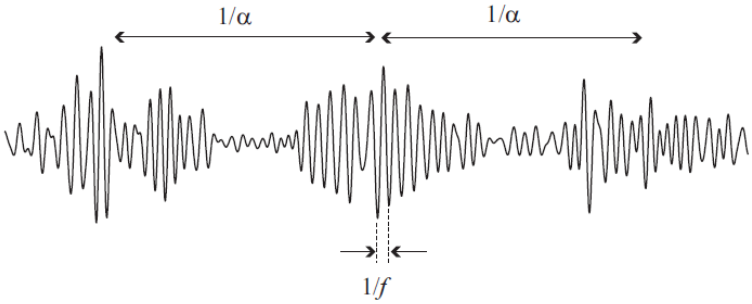

Figure 25: Spectral frequency f and cyclic frequency α of cyclostationary waveform [image courtesy of (12)]

Considering the signal represented in Figure 25, it represents a cyclostationary waveform in terms of carrier and modulation frequency, where *f* is named *spectral frequency* and it is the carrier frequency of the signal, while the cyclic frequency α is the modulation frequency. Obviously, the modulation frequency of a signal is always lower than its carrier frequency ($\alpha < f$). This signal is the equivalent of that emitted by a fault in a bearing, where the cyclic rate represents the periodicity with which the shock repeats over time.

To visualize the hidden periodicities in a signal, we can introduce the *spectral correlation density*, a tool that allows to display the signal simultaneously in time and frequency domains. The starting concept consists in decomposing the energy flow of the signal into periodic components which represent how the energy varies over time **(12)**. The mean instantaneous power is defined as:

$$\boldsymbol{P_x(t) = \mathcal{P}\{|x(t)|^2\}}$$

It provides a view of how the energy of a signal flows over time, revealing any periodicity. However, to see how the mean instantaneous power is distributed at the same time in the frequency and time domain, it is necessary to apply a band-pass filter, Δf width, centered on a frequency *f*, to the signal $\boldsymbol{x(t)}$. In this way the mean instantaneous power passing through a given frequency band is obtained. By applying a series of band-pass filters, known as a filter bank, to the signal, the instantaneous power spectrum is obtained, as shown in Figure 26. To quantify the intensity of these periodicities, Fourier analysis is applied to the instantaneous power spectrum, obtaining what is called the *cyclic modulation spectrum*, as a function of the spectral frequency f and the cyclic frequency α. When read along the α-axis it is like an amplitude Fourier spectrum characterizing the cyclic frequency of the signal, while on the *f*-axis it is a Power Spectral Density. If any spectral band is detected on the α axis of the spectrum, some

cyclostationary component is present in the signal. On the contrary, a stationary signal has all its energy distributed only along the *f* axis, i.e. for α= 0. **(13)**

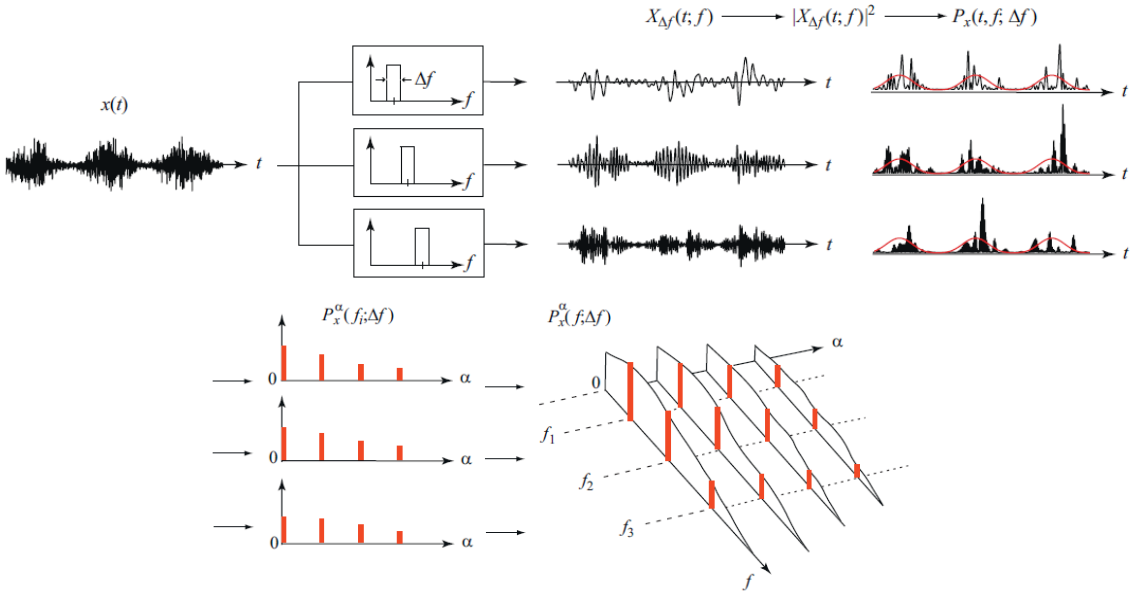

Figure 26: Interpretation of instantaneous power spectrum and cyclic power spectrum [image courtesy of (12)]

An evolution of this tool is represented by the *spectral correlation density*, a correlation density between two spectral components spaced by α around the frequency *f*. Without going into too much detail on the subject, the main difference with the cyclic modulation spectrum is that the latter is a power expressed in W, while the spectral correlation density is a density, therefore expressed in W/Hz. However, it is important to underline that they are both functions of the same frequency variables and both show the presence of a modulation in a signal with cyclic frequency α as a function of the spectral frequency *f*. By normalizing this density with respect to the energy of the signal, to eliminate the scale effect, the *cyclic spectral coherence* is obtained.

An example of a signal coming from a gearbox with a defective bearing analyzed with the spectral correlation density (a) and the spectral coherence (b) is shown in Figure 27. In the spectral correlation density, there are a series of spectral bands on the α cyclic frequency axis, below the spectral frequency *f* of 6 kHz. These are due to the periodic rotation of the gears in the gearbox, which produce a first order cyclostationary signal. As previously discussed, this signal is very intense, therefore it tends to drown out other weaker signals from the gearbox, such as those from the defected bearings. The spectral coherence in Figure 27 (b), being a "relativized" measure with respect to energy, is able to highlight even those weaker cyclostationary components. In this case there is a

distribution of spectral bands above 6 kHz spaced by 30 Hz, indicating a second order cyclostationarity due to a defect on the bearing outer race **(12)**.

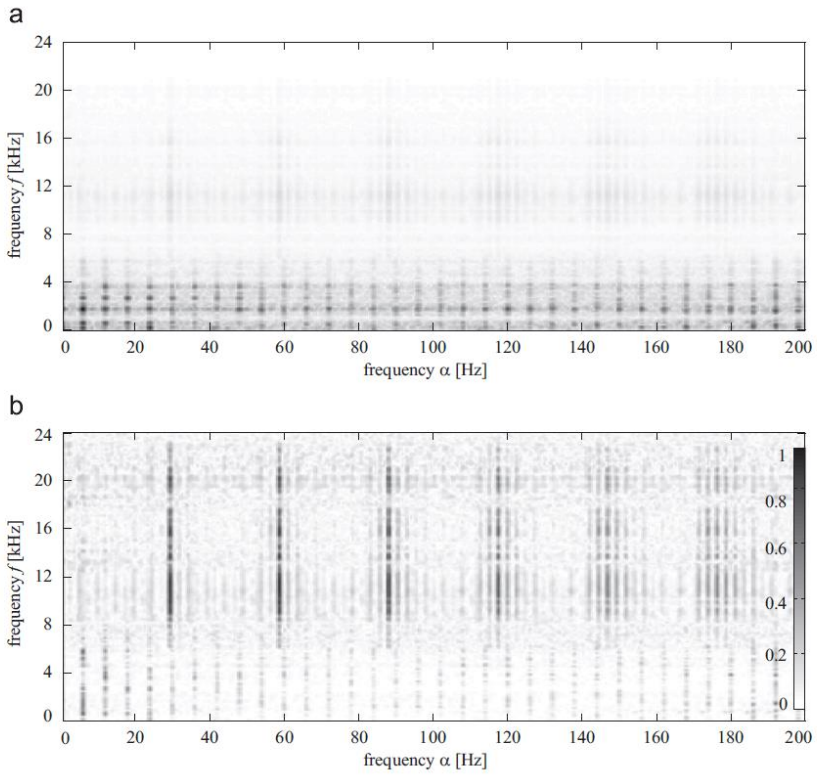

Figure 27: Example of analysis with spectral correlation density (a) and spectral coherence (b) of the vibration signal of a gearbox with defective bearing. [image courtesy of (12)]

4. The proposed method

Continuous monitoring of some vibrational parameters makes it possible to identify a sudden change in the operating condition of the machine under test and trigger an alarm, if necessary. However, as previously discussed, this type of analysis does not allow to identify the type, severity and location of the damage, in this regard the algorithms chosen for the analysis are introduced.

After careful bibliographic research among the different signal processing techniques, it was learned that most of the successful techniques for bearings damage detection focus on the vibration signal separation in the corresponding issued by the different sources. This separation can be accomplished by exploiting the characteristics of the signals emitted by gears and bearings, corresponding respectively to the deterministic/non-deterministic contributions.

One of the most used methods to obtain this separation is the Synchronous Average, an algorithm which consists in averaging the vibrational signal acquired over a certain number of revolutions of a reference shaft. To do this it is necessary to resample the acquired signal from the time domain to the angular domain, in such a way as to obtain an integer number of samples per cycle. This process is called Computed Order Tracking and it is discussed in detail in the following section.

After extracting the residual signal containing the indication of a possible damaged bearing and the noise, it is possible to analyze it using the diagnostic algorithms previously discussed. In particular, two methods are used and compared: Envelope Analysis and Spectral Coherence. The first it's used to demodulate the residual signal in amplitude and investigate the presence of the bearing's characteristic frequencies on the spectrum, after filtering the signal, in the band identified by the Fast Kurtogram algorithm. While the second, it's an algorithm find in literature, which is able to identify ciclostationary signals in a high level of stationary noise.

A complete method for vibrational analysis is proposed in this chapter, which allows to isolate the residual signal and to analyze it with the previously discussed diagnostic algorithms.

4.1. Computed Order Tracking and Synchronous Average

The order domain analysis is a frequency analysis method that uses multiples of the running speed, called orders, instead of the frequency in *Hz*. **(14)** Order tracking links the vibrational signal to the rotational speed of the shaft, allowing the vibrational contents proportional to the rotational speed to be identified more easily in the

spectrum. To use this kind of analysis, it is necessary to sample the vibration signal at constant angular increments of the shaft. This usually it's done in postprocessing, where the Computed Order Tracking (COT) is used to resample the signal acquired at a constant frequency ($\boldsymbol{f_s}$), in time domain, to constant angular increments of the shaft ($\boldsymbol{\Delta\theta}$). In this way, with this process also known as "angular resampling", a signal is sampled with an integer number of samples per revolution, called Samples Per Cycle (SPC), at a rate proportional to the shaft speed. SPC is therefore the analog of the sampling rate of the frequency domain in the angular domain.

To extract the trend of the angular position as a function of time, an analog instrumentation is used to obtain the so-called *tachometer* signal, usually acquired via an optical sensor and a phonic wheel (keyphasor) integral with one shaft of the machine. From the tachometer signal can be obtained the angular velocity signal, by calculating the vector of the time instants in which a reference on the shaft passes in front of the optical sensor, thus obtaining a 0-1 square wave signal.

The resample process occurs in two different steps. The first, involves the determination of the resample times. Assuming that the shaft is undergoing constant angular acceleration, the shaft angle equation can be obtained considering the following quadratic law of motion:

$$\boldsymbol{\theta(t) = b_0 + b_1 t + b_2 t^2}$$

The coefficients $\boldsymbol{b_0}$, $\boldsymbol{b_1}$ and $\boldsymbol{b_2}$ can be found by fitting the angular signal as function of time at known shaft angular increments. To obtain uniform angular sampling, the resampling of shaft angle is performed considering:

$$\boldsymbol{\theta(t) = k\,\Delta\vartheta}$$

where $\boldsymbol{\Delta\vartheta}$ is the desired angular spacing between two consecutive pulsations, that can be computed given the number of SPC.

$$\boldsymbol{\theta(t) = k\frac{2\pi}{SPC} = k\,d\theta}$$

Once the angular sampling has been defined, the corresponding resample times are obtained from the inverse equation of the function $\boldsymbol{\theta(t)}$, so the resampling equation becomes:

$$\boldsymbol{t(\theta) = \frac{1}{2b_2}\left(\sqrt{4b_2(k\,\Delta\vartheta - b_0) + {b_1}^2} - b_1\right)}$$

In the second step, the new time axis can be used to obtain the corresponding amplitudes of the signal, that are calculated by interpolation of the original signal (spline interpolation). A function has been implemented in *MATLAB®*, to compute this resampling process, given as input the signal to be resampled, the original sampling rate, the tachometer time impulses and the number of SPC. This last parameter is decided after calculating the number of SPC of the original signal, with reference to a shaft of the machine, as follows:

$$\boldsymbol{SPC = \frac{Signal\ samples}{Shaft\ revolutions}}$$

Obviously this number very hardly is an integer, therefore the number of SPC that will be used in the COT will be rounded to the nearest integer.

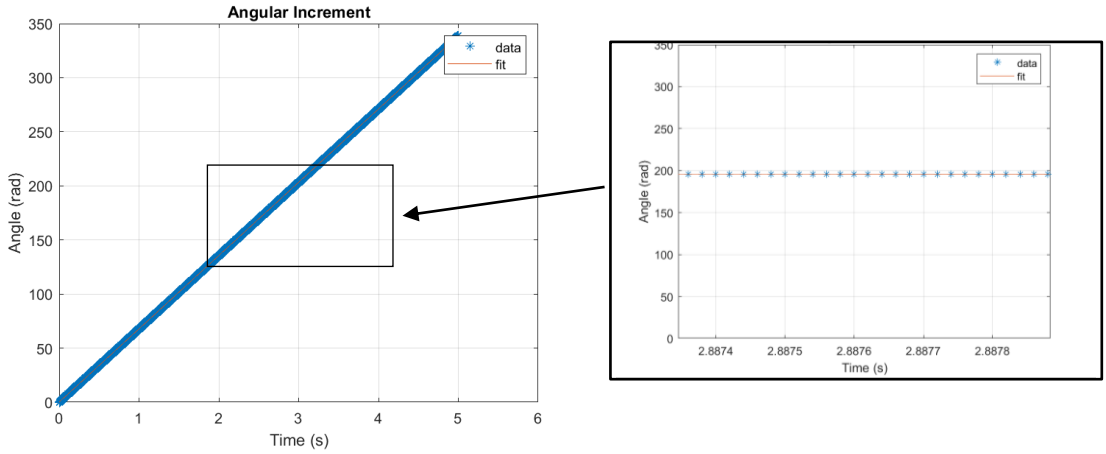

Figure 28: Angular increment interpolating function

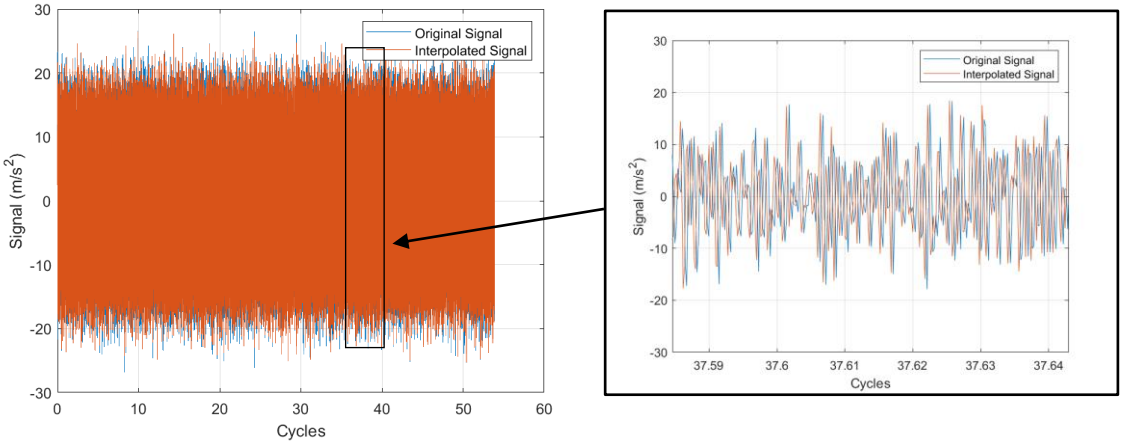

Figure 29: Original vs Interpolated signals

Time Synchronous Average (TSA) is a signal processing technique able to separate the periodic waveform from the background noise of a signal. **(15)** It is one of the most used algorithms for gearbox analysis, where it allows to separate the vibration signature of a gear with respect to other gears and noise which includes also the cyclostationary signal of the bearings. Having resampled the signal based on constant angular increments, the algorithm that best suits our case is the Synchronous Average (SA), i.e. the equivalent of the TSA in the order domain.

As referred in the following formula, the periodic signal is obtained by averaging a series of segments of the resampled signal, each corresponding to a complete revolution of the gearbox shaft chosen as a reference.

$$\boldsymbol{y_a(t) = \frac{1}{N} \sum_{n=0}^{N-1} y\,(t + nT)}$$

It is important to note that the COT, as a step prior to the application of the SA, is essential to obtain good results. This is because, each signal segment to be averaged must have a finite number of samples per rotation of the gearbox shaft, in order to have exact correspondence between consecutive sections. In this way, the harmonics of rotation of the gear corresponding to the reference shaft can be determined with the synchronous average of the different segments of the signal. At this point, having obtained the synchronous signal on one revolution of the shaft, this can be repeated for the number of revolutions to obtain the corresponding periodic signal with the same time duration as the original signal. The residual signal can be obtained simply by subtracting the periodic contribution from the original signal.

In the following figures it is shown the application of SA algorithm, implemented in *MATLAB®*, to a vibrational signal used to test the algorithm. The COT algorithm was applied using as a reference for the angular resampling the tachometer signal acquired with an optical sensor from a phonic wheel, from which it was possible to obtain the angular velocity information. Subsequently, the SA algorithm was applied to the vibration signal thus obtaining the corresponding periodic contribution due to the meshing gears and electric machines.

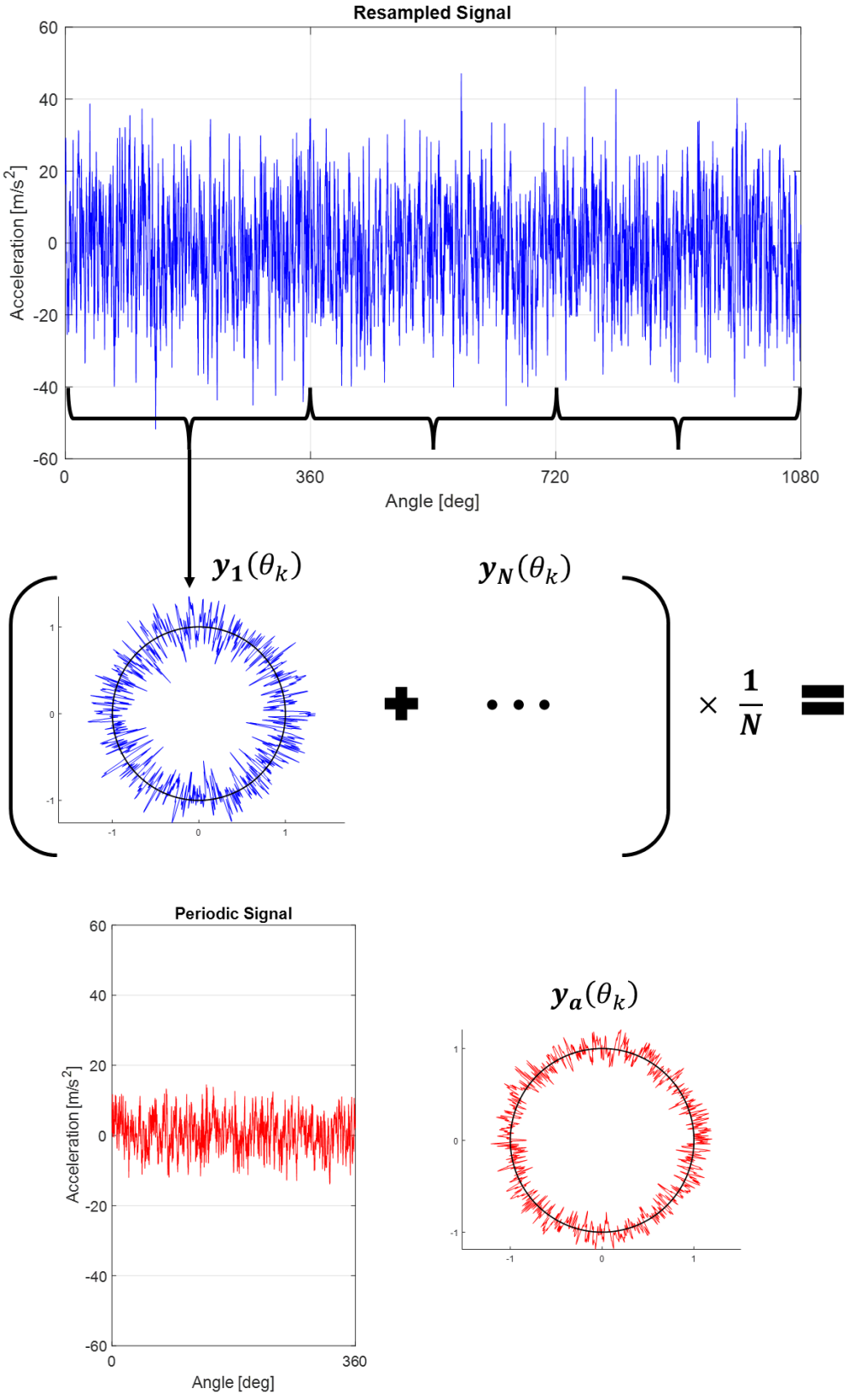

Figure 30: Synchronous average explained graphically

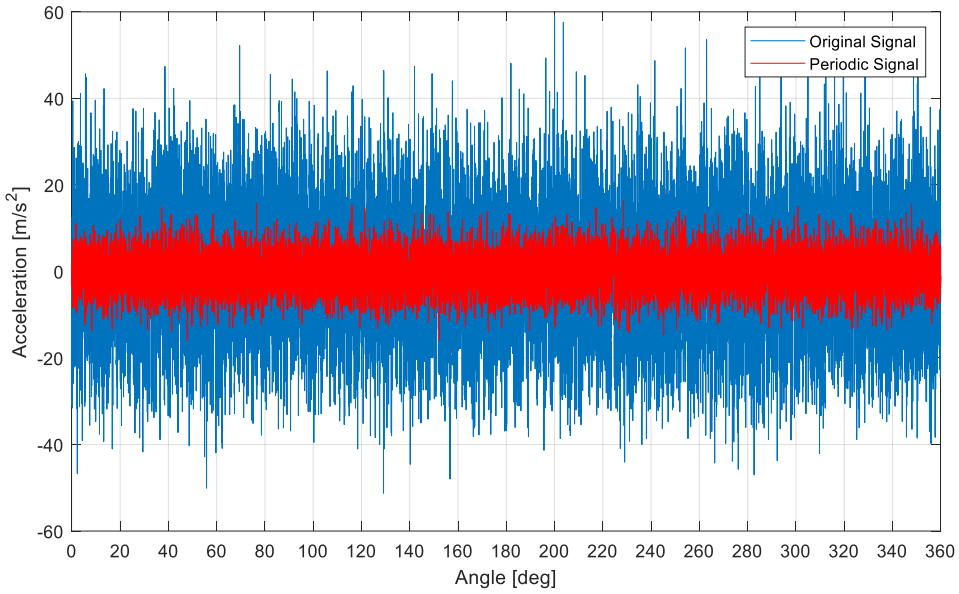

Figure 31: Original and Periodic signal (SA Signal) over one shaft revolution

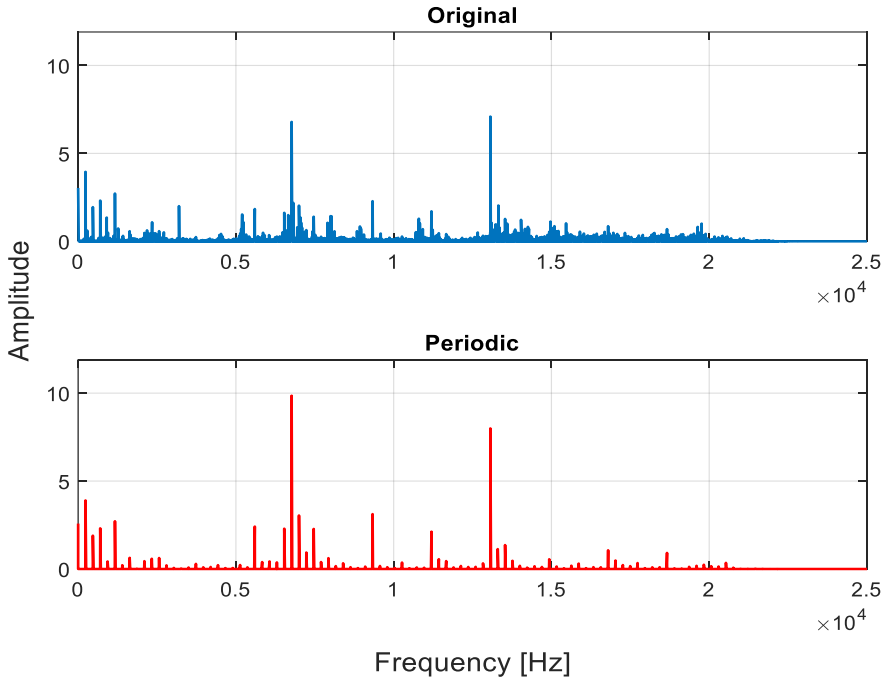

Figure 32: Frequency spectrum comparison between Original and Periodic signal

As can be seen from the spectrum (Figure 32), only the periodic components of the signal appear in the spectrum of the periodic signal, i.e. those referring to the orders of rotation and the GMF (gear-mesh frequency) of the meshing gears on the reference shaft. Therefore, it can be seen that the efficiency of the algorithm in separation is

considerable, but its efficiency is limited by the fact that the entire procedure must be repeated for each shaft present in the gearbox. Considering a multi-stage complex gearbox with several shafts and gears, the method to extract the periodic contribution of each of them consists in applying the COT + SA algorithms in sequence on each shaft. In other words, once the residual signal has been obtained with respect to one shaft of the gearbox, this signal has to be re-sampled to have an integer number of samples per period with respect to the n^{th} shaft and used to extract the corresponding periodic contribution. By following this procedure iteratively for all the shafts of the gearbox, the last residual is obtained containing only the contribution of the bearings and the background noise.

4.2. The bearing diagnostic procedure

The main purpose of this vibration analysis is to identify a possible defect in the bearings of the e-Axle in the endurance test, before it manifests causing permanent damage to further mechanical and/or electrical components.

To achieve this goal, it is necessary to extract the weak vibration signature produced by bearing faults from the global vibration signal, which is acquired, via accelerometers, in different locations on the e-Axle cover. As previously described in chapter 3, the vibrational signal contains both the deterministic part, mainly due to the gear mesh, and the random part, related to other phenomena such as bearing operation. The deterministic part, as we have seen, can be obtained from the original signal by applying the Synchronous Averaging (SA) algorithm, after first resampling the signal in constant angular increments with the Computed Order Tracking (COT) algorithm. By applying this procedure in cascade for each shaft, the non-deterministic part of the vibration signal can be isolated, enhancing in this way the bearing signature. **(16)**

This procedure has been implemented in *MATLAB®*, with iterative loops that repeat for input, intermediate and output shaft of the e-Axle. Subsequently, the last residual signal obtained is processed by the bearing diagnostic algorithms, previously discussed. The reference method is the Envelope Analysis, which allows to demodulate the signal after filtering it in a frequency band, selected by the Fast Kurtogram algorithm, and to detect bearing fault frequencies with frequency analysis. An alternative algorithm, the Spectral Coherence is proposed, a tool used to characterize ciclostationary signals hidden in a high level of stationary noise.

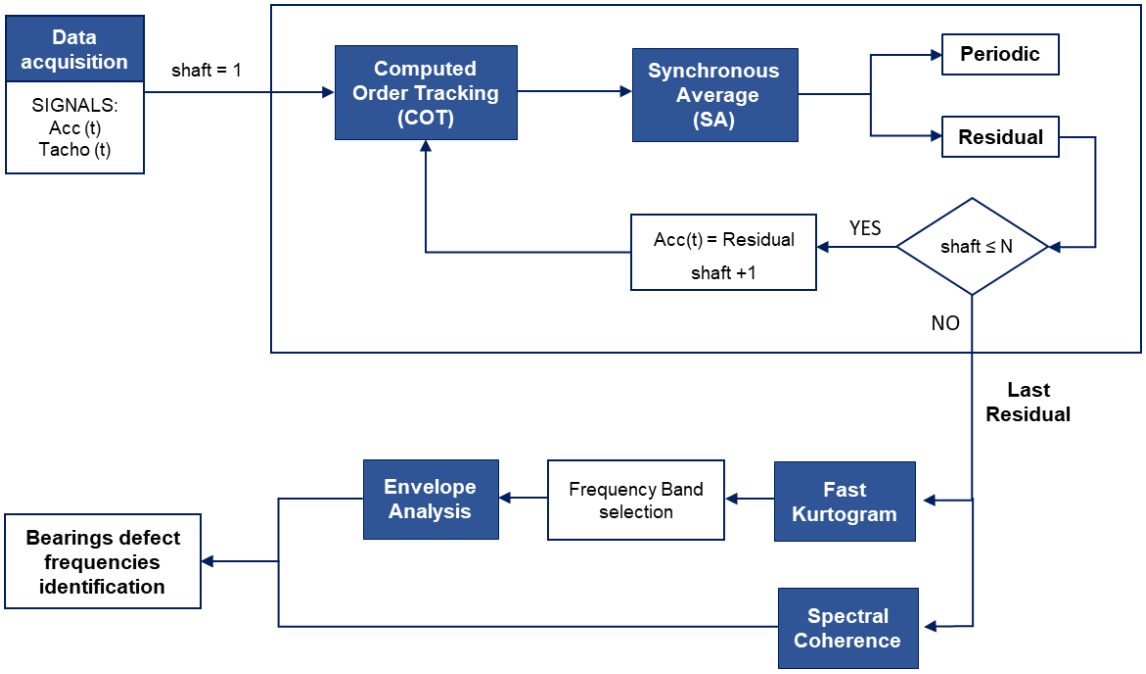

Figure 33: Blocks diagram of the procedure for detecting bearing damage

The residual signal as definition in chapter 3, is calculated after each iteration by subtracting the periodic signal obtained from the Synchronous Average from the original interpolated signal in the time domain.

The following figure shows the spectrum in orders referred to the input shaft of the respective signals obtained by applying the procedure to a vibrational signal acquired on the e-Axle, starting from the input shaft. The residual signal in the bottom right plot in Figure 37 is the Last Residual depurated of all deterministic contributions, i.e. the periodic signals of all the three shafts. This Last Residual signal will be processed by the diagnostic algorithms to detect if any fault is present in the rolling bearings.

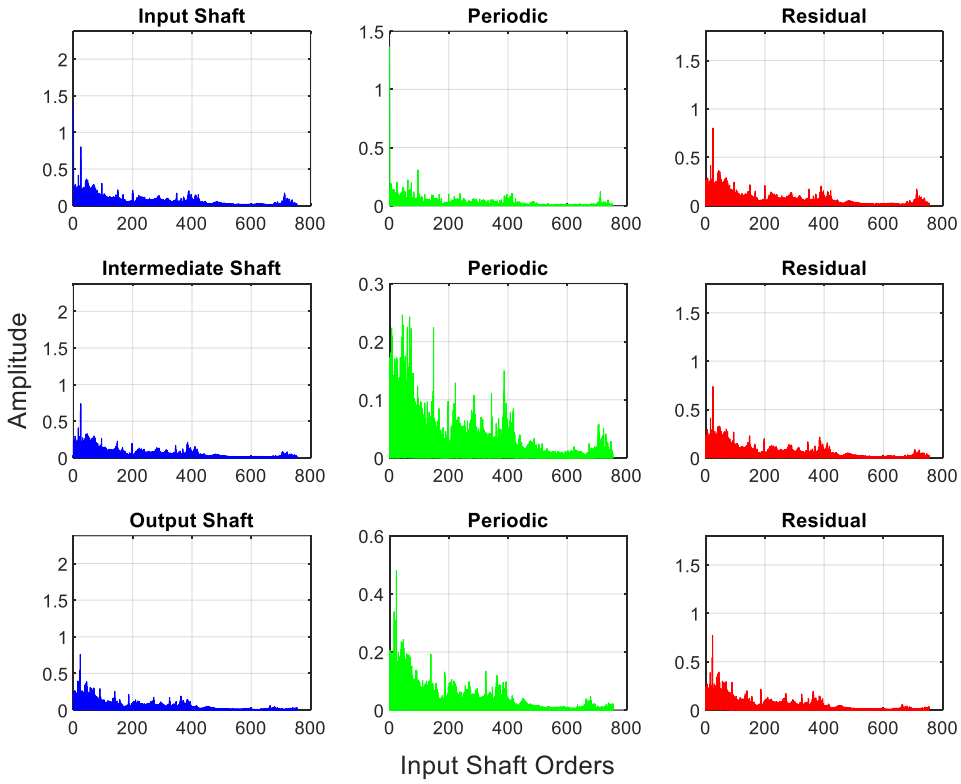

Figure 34: Input shaft orders spectrum obtained from the procedure

4.3. Analysis of defected bearing signals

To test the effectiveness of the algorithms described in chapter 2 in diagnosing defects in rolling bearings, real vibration signals containing a known defect were analysed.
The two signals analyzed were acquired at the sampling frequency $\boldsymbol{fs = 44100\ Hz}$ and are characterized by the following defects:

- Signal 1: Defect on the inner race
- Signal 2: Defect on the outer race

The ball bearing has the characteristic frequencies shown in the table.

f_r	29.5 Hz	Inner ring speed
BPFI	147.9 Hz	Ball pass frequency inner ring
BPFO	88.06 Hz	Ball pass frequency outer ring

Table 10: Bearing characteristic frequencies

For each of the signals the Fast Kurtogram is calculated, using the respective function in *MATLAB®*, then a band-pass filter was applied to the signal and the envelope spectrum was obtained.

As can be seen from the Figure 35, analyzing Signal 1 with defect on the inner ring, the maximum value of kurtosis detected by the algorithm is in correspondence of the central frequency f_c equal to 2756.25 Hz and level 3.5. By filtering the signal, on the corresponding envelope spectrum in Figure 36, it is possible to identify the characteristic frequency of the defect (BPFI = 148 Hz) and its harmonics.

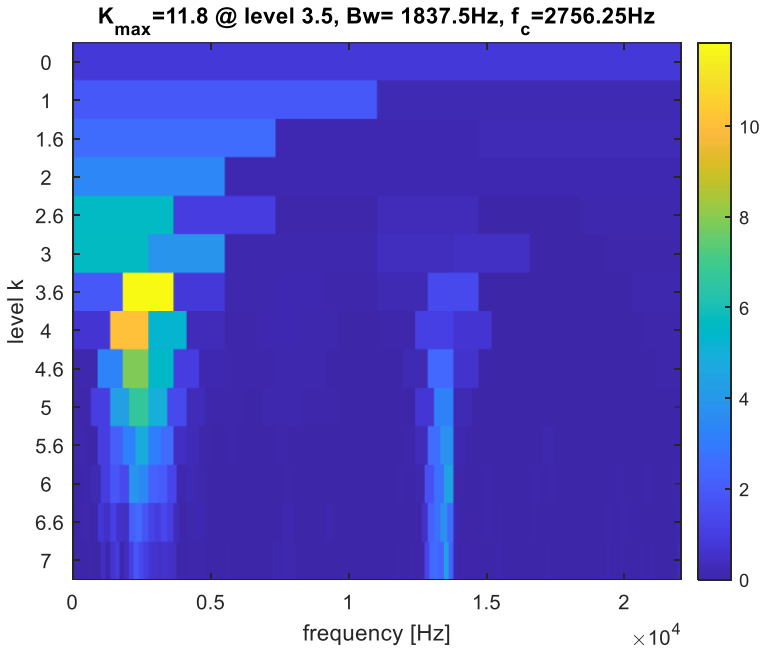

Figure 35: Signal 1: Fast Kurtogram

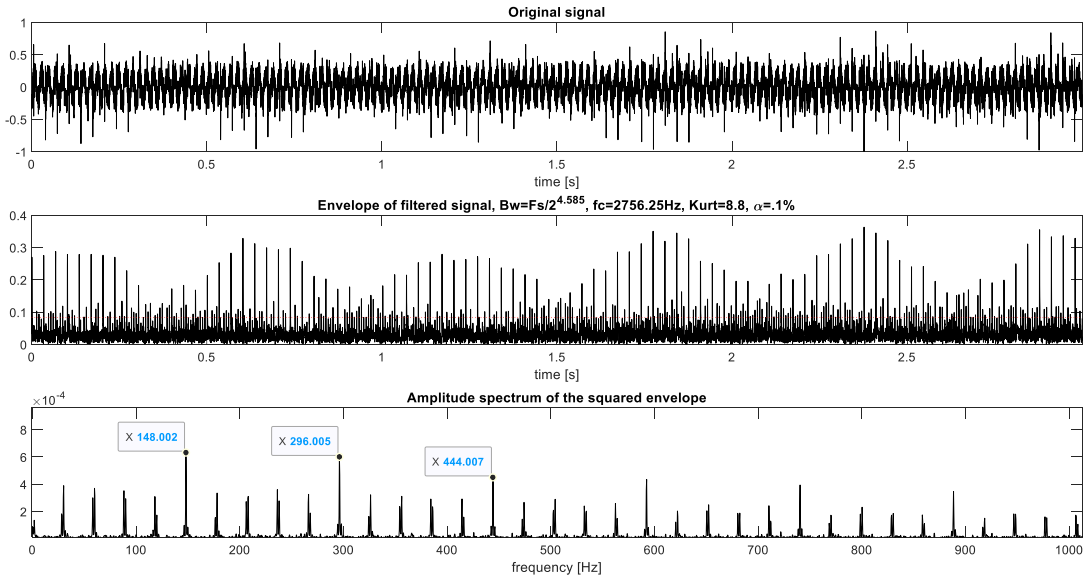

Figure 36: Signal 1: original signal, envelope signal and envelope spectrum for fc = 2756.25 Hz

The same analysis is repeated on Signal 2, in which the maximum value of kurtosis is identified in correspondence with the central frequency f_c = 13522 Hz. Filtered the signal in correspondence of the band identified by the FK corresponding to level 7, the envelope spectrum is obtained in Figure 37 from which, however, it is not possible to identify any characteristic frequency of the bearing. Therefore, analyzing again Figure

37, we can note that another band also has a rather high level of kurtosis, therefore we decide to repeat the analysis by filtering the signal at the central frequency f_c = 2067 Hz and level 4. It is now possible to easily identify on the envelope spectrum in Figure 39 the characteristic frequency of the inner ring defect (BPFI = 91 Hz) and its harmonics.

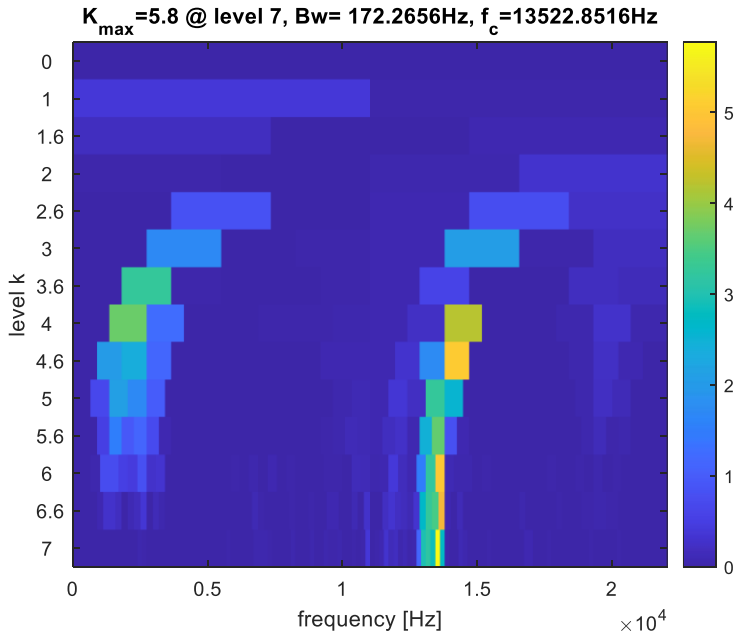

Figure 37: Signal 2: Fast Kurtogram

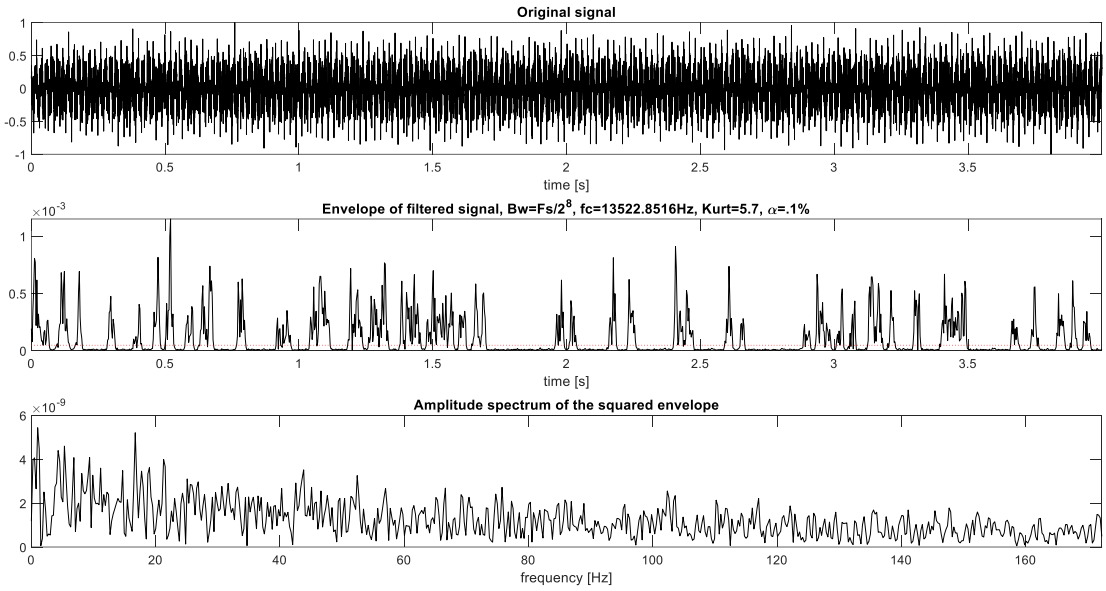

Figure 38: Signal 2: original signal, envelope signal and envelope spectrum for fc = 13522 Hz

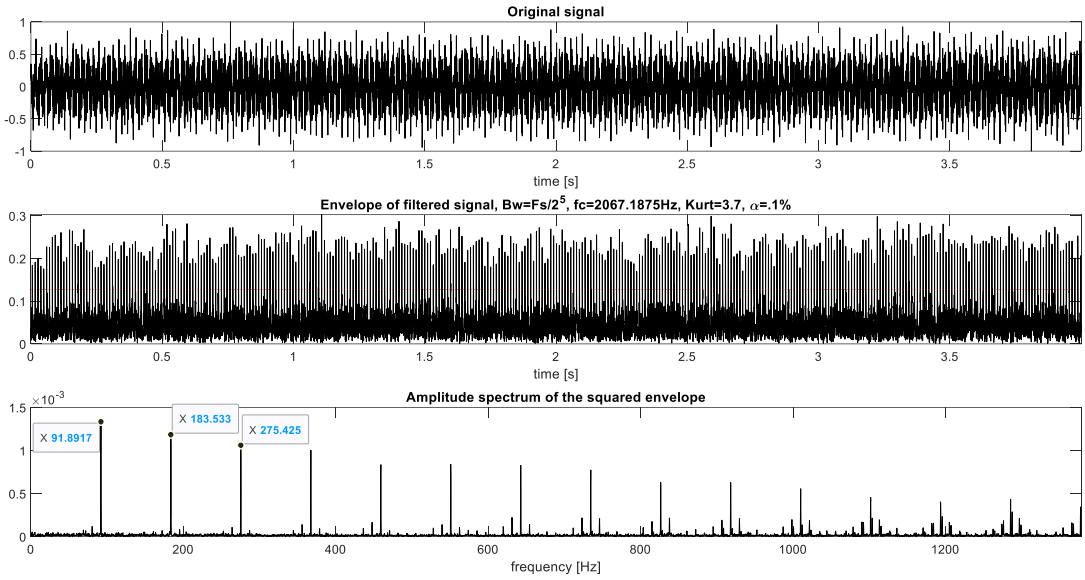

Figure 39: Signal 2: original signal, envelope signal and envelope spectrum for fc = 2067 Hz

This highlights a problem of the Fast Kurtogram in identifying, unequivocally, the correct band for signal filtering. In fact, it can be noted that the algorithm recommends applying a band-pass filter in a rather narrow frequency range (f_c = 13522 Hz, Bw = 172 Hz, level 7) as it detects the highest kurtosis value. However, this phenomenon is not said to be related to a defective bearing, but to other impulsive phenomena which cause outliers in the acquired signal. This underline the necessity to preprocess the vibration signal to eliminate all the contributions that are not directly related to a bearing signature.

However, it can be concluded that EA together with FK, has successfully extrapolated the characteristic frequencies of the defects in the bearings, but it should be emphasized that this is possible only as long as the defect is punctual and localized.

.

5. Experimental test

5.1. Test bench overview

A transmission dynamometer, also called “dyno”, is used in the automotive industry to validate durability and mechanical integrity of a gear set **(4)**. A traditional test bench used for testing and homologation of complete driveline systems, composed by a driving shaft, a differential gear set and two driven shafts, it’s composed of 3 independent electric motor/generator dynamometers, one connected to the input shaft of the transmission, also called propeller shaft, and the other two flange mounted directly to the driveshafts of the driveline in place of the vehicle wheels. Either AC motors or DC motors can be used as adsorption/driver unit and they act as motor when they drive the system under test, while they act as generator when they are driven. When a dyno is used as absorbing dynamometer, it acts as a load that is driven by the Unit Under Test (UUT) and so by the prime mover and regenerate DC electric energy that can be returned back to the commercial electric power grid using a DC/AC converter. **(17)** Each dyno unit is equipped with two types of control systems that have to perform different tasks: a speed regulator allows to control the amount of braking torque that is necessary to maintain a certain constant level of speed of the prime mover, while a braking torque regulator is used to provide a certain level of braking torque while the prime mover operates at the desired speed. Therefore, given a specific set of torque and speed, the automation system sends the information to the electric machine that, with a PID controller, reach the desired condition of speed/torque. The dynamometer connected to the propeller shaft usually it is controlled in torque, while the other two dynamometers connected to the driveshafts are controlled in speed.

The configuration of the test bench used to perform the endurance test of the e-Axle is slightly different from which explained above. In order to simulate the road load- of the vehicle drivetrain on the two shafts of the e-Axle, only two independent dynamometer units are needed, since the prime mover, unlike a traditional driveline, are the two electric motors of the e-Axle.

The dyno test setup is undoubtedly the part that has brought about the most changes compared to a test of a conventional driveline. It was necessary to introduce new systems capable of supplying high voltage electricity to power the electric motors, new measuring instruments and also different safety systems. Furthermore, a cooling circuit is also necessary to cool the e-motors and inverters, in conditions similar to those

in vehicles, but with the difference that the cooling of the coolant in this case is managed by a liquid/liquid heat exchanger instead of a radiator. The next paragraphs provide an overview of the test bench layout and the sensors used to monitor the test.

5.1.1. Layout and measuring equipment

The test bench considered to run the e-Axle endurance test is composed of two dynamometer DC electric motor with an adaptation transmission (gearbox) for each of them. These adaptation units adjust torque and speed on the two axles output dyno for the specific application using 3 gear ratios for respectively low, high and direct speed application; for this test it is set to direct speed configuration. The output torque and speed of the UUT is measured by torque meters mounted on the adaptation unit output shafts and connected to the wheel flanges of the UUT by cardan shafts. Figures 40-41 shows a sketch of the test layout. The technical data of the test bench main components are:

Output Dyno:

- Power Max: 1000 kW each machine
- Torque Max: 26 kNm each machine
- Wheel Speed Max: 1500 rpm

Reduction Unit:

- Direct drive: Ratio 1:1

Torquemeter:

- Torque Range: ± 20000 Nm

Battery Emulator (DC source):

- Voltage Max: 1200 V
- Current Max: ± 1200 A
- Power Max: 1000 kW

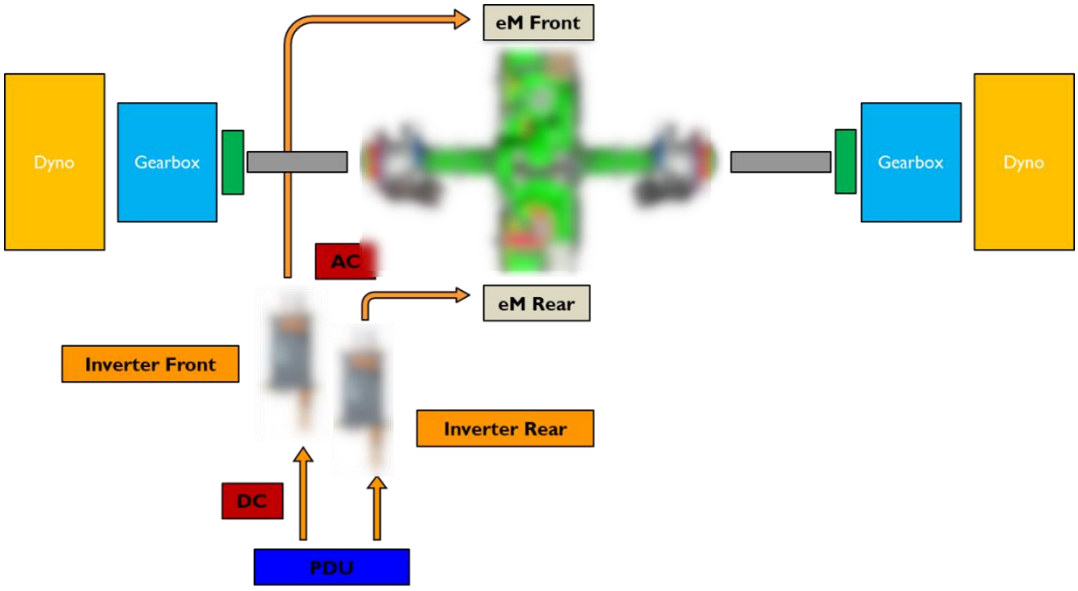

Figure 40: Sketch of test bench layout (upper view)

Figure 41: Sketch of test bench layout (front view)

Cooling circuit

The cooling circuit is used to cool the stators of the electric motors and the inverters. A fixed displacement pump supplies a flow rate of refrigerant fluid which, after being cooled in a liquid/liquid heat exchanger, is distributed to the respective components.

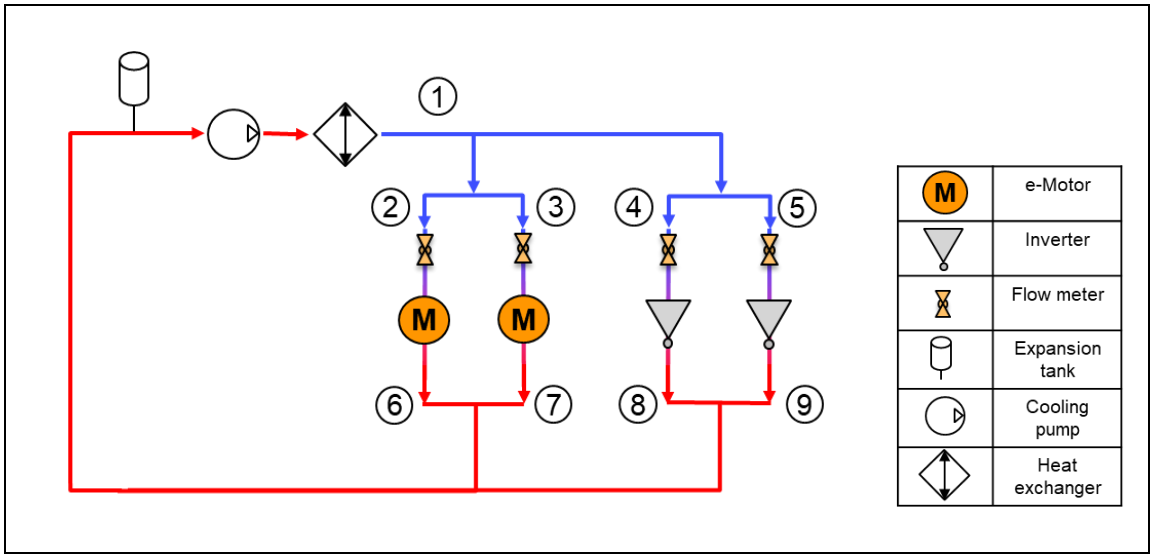

Figure 42: Cooling circuit

To monitor the operating conditions during the test, pressure, temperature and flow rate are measured in the various sections of the circuit. With reference to Figure 42, the following table shows the measured quantities in correspondence of the indicated numbers.

ID	Sensor Description	Unit
1	Coolant delivery temperature	°C
	Coolant delivery pressure	mbar
2-3-4-5	Coolant delivery flow rate	l/min
6-7-8-9	Coolant return temperature	°C

Electrical circuit

To develop the bench test it is necessary to power the electric motors in a condition similar to the real operating one, however rather than using a real battery, a battery emulator is used to simulate the battery's characteristics. For testing purpose, this system allows to dramatically reduces test time, since normally it takes several hours to fully charge a real battery, instead this system allows to quickly vary the voltage to simulate the battery characteristics on a real vehicle. The most important property of this system, in comparison to a conventional power supply, is their ability not only to source DC current but also to sink current since it is a bidirectional power supply system. This is fundamental to perform the test, since when the e-Motors are in regenerating phase, they generate electric energy that “charge” the battery emulator. A battery emulator system provides also highly repeatable test results since it eliminates the

variable of battery temperature or aging that can influence the test result, reduce energy consumption and creates a secure testing environment, preventing risks of exposure to dangerous gases or explosions that can arise with the use of real batteries.

The electric circuit mainly consists of two parts: one with high voltage and the other with low voltage. The high voltage circuit is the power supply circuit of the e-Axle, comprising the direct current (DC) section between the power source, in this case the battery emulator, and the inverters. Next, the inverters transform the DC current into alternating current (AC) to power the electric motors of the e-Axle.

It is important to note that the main "novelty" in the test setup concerns the high voltage electrical circuit, since new safety and control systems are required.

Figure 43: High Voltage Bench Electric connection

Instead, the low voltage circuit concerns the control part of the inverters and their interface with the Transmission Control Unit (TCU) and the computer control software in the control room.

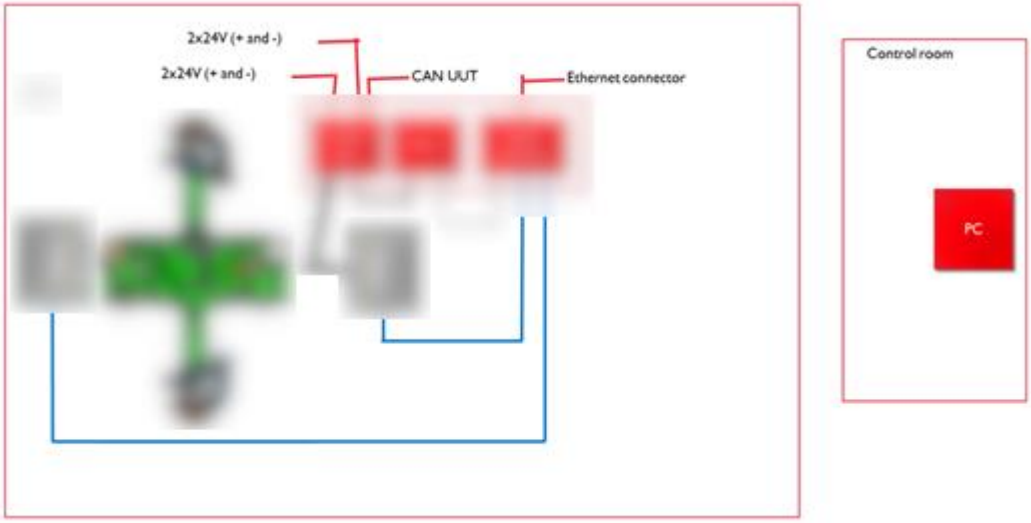

Figure 44: Low Voltage Bench Electric connection

5.1.2. Data acquisition system and sensors

The test bench is equipped with a computer system provided for:

- The control and monitoring of test.
- The low/high speed acquisition and storage of test data such as speed, torque, temperatures, pressures, High Voltage (HV) currents (DC/AC) and internal CAN variables of the e-Axle control unit.

The test bench acquisition system is featuring analogue and digital input channels. In addition, the computer has one CAN-bus module, capable of continuously reading, processing and storing data from the CAN bus of the transmission control module. The dynamometer control system is implemented on the automation software that can run test cycle by setting the set-point of torque and speed. To prevent a fatal damage of the test transmission during the durability cycle, critical signals such as temperatures, pressures and vibrations are automatically monitored to trigger test bench safety shut-down procedures, based on certain limit thresholds.

The test bench is equipped with a second computer system for the high-speed data acquisition. Usually, the most common transducer used to acquire the vibration signals is the accelerometer, such as the one in Figure 45. The piezoelectric accelerometers originates a signal proportional to the acceleration measured, thanks to a sensing element made of piezoelectric material, that emits a charge when subjected to a compressive force from an inertial mass. The sensing element is housed in a sensing body, usually made in stainless steel and can be fixed to the support with hard glues or magnetic mounts. **(18)**

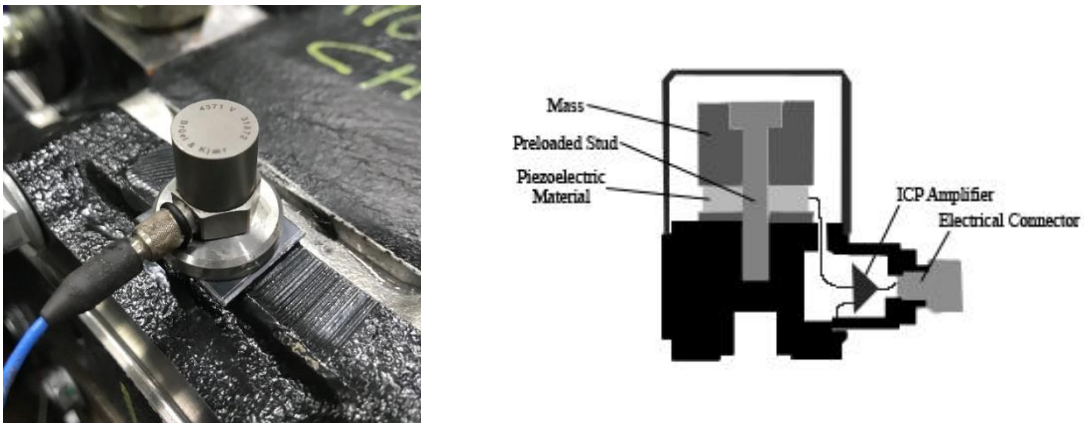

Figure 45: A piezoelectric accelerometer and its internal components

Company	Model	Type	Reference sensitivity [pC/g]	Upper Frequency Limit [kHz]	Resonance Frequency [kHz]
Brüel & Kjær	4371 V	monoaxial	9.39	12.6	39.9

Table 11: Technical characteristics of the accelerometers used for signals acquisitions.

The technical characteristics of the accelerometers used in this test are presented in Table 11. They are fixed with the magnets in various positions on the e-Axle case and connected with low noise shielded cables to the acquisition unit, on six different channels, as shown in Figure 46. Channels 1 and 2 measure the vertical acceleration on the e-Motor covers, in correspondence of the bearings supporting the primary shafts and the rotors. Channels 3 and 4 acquire vertical acceleration on the e-Axle case, in correspondence of the bearings supporting the gearbox secondary shafts, while channels 5 and 6 are recording of the acceleration on the bearings supporting the primary shafts on the transmission side (Table 12).

All the accelerometers' channels are connected to the *AVL X-ion™* data acquisition system, which is able to sample up to 32 channels at the same time. The system could be set to measure a certain number of seconds of time for each channel and to start the measurement event if a certain condition is met. In this case, a measurement condition has been defined as a function of the torque value detected by the torquemeter. The data is then saved in the PC memory and can be exported and converted into various formats for postprocessing.

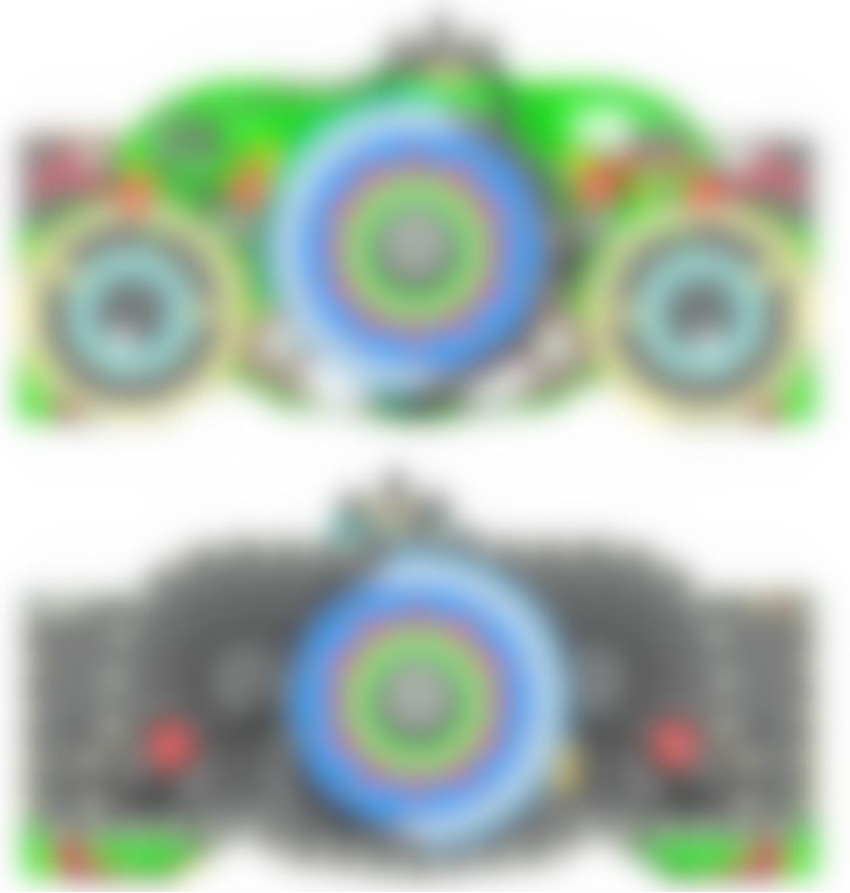

Figure 46: Position of the 6 accelerometers on the e-Axle cover

Channel name	Position	side
chan1	Front e-Motor cover – vertical	eDrive
chan2	Rear e-Motor cover – vertical	eDrive
chan3	Front intermediate shaft – vertical	eDrive
chan4	Rear intermediate shaft – vertical	eDrive
chan5	Front input shaft	Transmission
chan6	Rear input shaft	Transmission

Table 12: Channels name and accelerometer position

5.2. E - Axle Vibration analysis

The signals analyzed in the previous section, relating to defects on the rings of a bearing, are certainly characterized by a lower level of complexity than those generated by a component such as an e-Axle. In fact, in these there was only the modulation due to the defect which allows an analysis of the signal without the use of particular

preprocessing methods, successfully diagnosing the cause of the defect. Under normal e-Axle test conditions, the acquired signal is highly influenced by various sources; both external to the component, due for example to the dynos of the test bench, but also internal, due to the strong masking of signals coming from the gears, electric motors and from the inverters. Therefore, the overall vibration signal is made up of the overlapping of the contributions of the different components and this makes it very difficult to diagnose defects in rolling bearings, which emit a much weaker characteristic signal than all the others. It is therefore necessary to apply the signal processing algorithms already described in Section 4.2 to the signal acquired during the test, in order to decompose it into the parts of interest.

5.2.1. Gearbox orders calculation

The initial goal is to analyze the signals and correlate the frequencies detected in the spectrum to the rotation orders of gearbox and the gear mesh frequencies (*GMF*) calculated. Below is the calculation of the *GMF* for the two reduction stages, being the gearbox symmetric, only one side is considered.

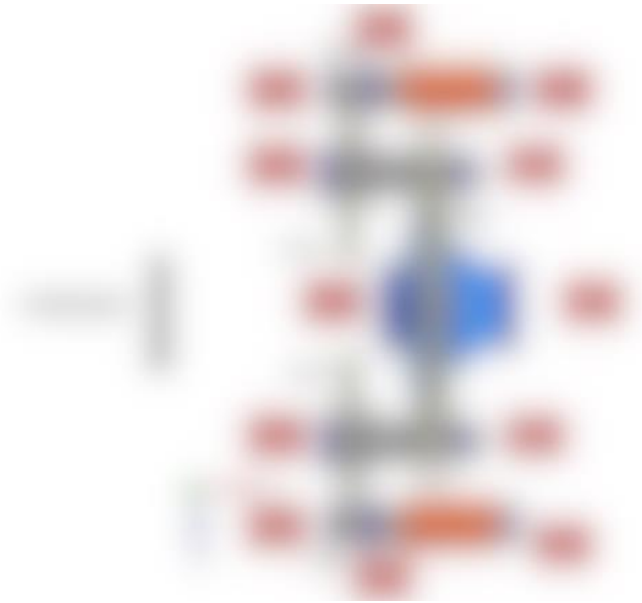

Figure 47: e-Axle mechanical layout

GEARS	STAGE 1		STAGE 2	
	Pinion	Gear Wheel	Pinion	Gear Wheel
Teeth Numbers				
Ratio				

Gear ratio	

Gears order referred to e-Axle INPUT shaft	
STAGE 1	
STAGE 2	

Table 13: e-Axle gear ratios and GMF

The transmission ratios for the two stages were obtained by dividing the number of teeth of the respective meshing gears. At this point, for simplicity in the analysis, it was decided to refer the meshing orders of the gears to the input shaft. Obviously, the order of the first stage is equal to the number of teeth of the pinion of the input shaft, while that of the second stage was obtained through the following relationship:

$$GMF_{stage2} = \frac{Z_{pin_{shaft2}}}{Ratio_{stage1}}$$

The e-Axle bearings characteristic frequencies are calculated using the formulas in section 3.3.3. and shown in Table 14 in rotation orders referred to the input shaft.

	INPUT SHAFT	
	Transmission side	e-Motor side
BPFI		
BPFO		
BSF		
FTF		

	INTERMEDIATE SHAFT	
	Transmission side	e-Motor side
BPFI		
BPFO		
BSF		
FTF		

	OUTPUT SHAFT	
	Transmission side	e-Motor side
BPFI		
BPFO		
BSF		
FTF		

Bearings orders legend	
BPFI	Ball / Roller pass frequency of inner ring
BPFO	Ball / Roller pass frequency of outer ring
BSF	Ball / Roller spin frequency
FTF	Fundamental train frequency

Table 14: Bearings orders referred to the e-Axle INPUT shaft.

5.2.2. Vibration signal feature monitoring

To monitor the test over time and to prevent test object fault, this data acquisition is used as an intermittent transient recorder. A measurement condition has been implemented in the acquisition software every time the torque value detected by the torque meter exceeds a certain value, i.e. every time the e-Axle works at maximum torque. In this way, the conditions of torque and speed are fixed and it's possible to monitor the test with high repeatability. An acquisition consists of 10 seconds of vibration signal recorded by the 6 channels of the various accelerometers at a sampling frequency of 50000 Hz. As previously described, during the recording, the torque and speed signals coming from the torque meters of the dynamometers are also acquired.

An acquisition of this data for each test cycle results in an impressive amount of data that must be acquired and stored for the entire duration of the test. To overcome this problem, the main goal was the creation of a database that allows to evaluate the evolution over time of the various indicators computed from the vibration measurements.

This post-processing was carried out in *MATLAB*® to compute the features described in section 3.4.1, capable of providing a general indication of the operating conditions of the e-Axle and on the presence of a damage. Eight features per each acquisition channel were then computed. Root mean square (RMS), mean value, peak to peak, shape factor, kurtosis, skewness, crest factor and impulse factor have extracted

for the acquisitions every 4 test hours and the corresponding extracted values are saved in a database.

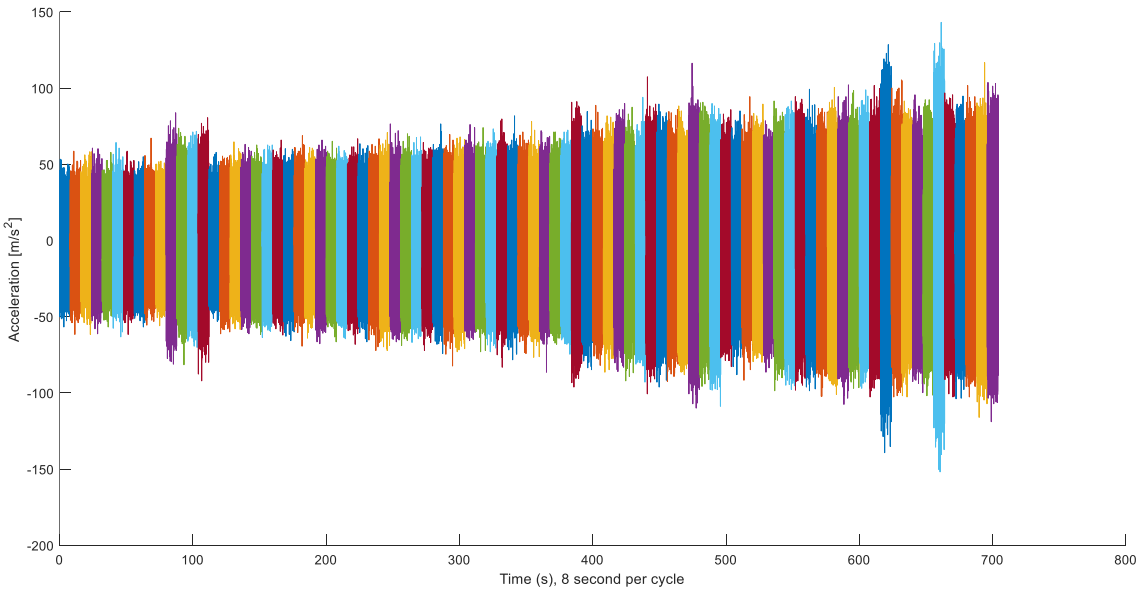

Figure 48: 8 s chunks of the original 10 s acquisitions every 4 hours of test execution.

In Figure 48, all the acquisitions of the raw vibrational signals relating to channel 1 are represented in sequence. As can be seen, the maximum amplitude has an increasing monotonic trend as the test progresses, with some outlines. This corresponds to expectations, since although the load and speed conditions are the same, the vibrational response of the e-Axle changes as the test progresses and normally the amplitude of the signal increases as all components are gradually worn out.

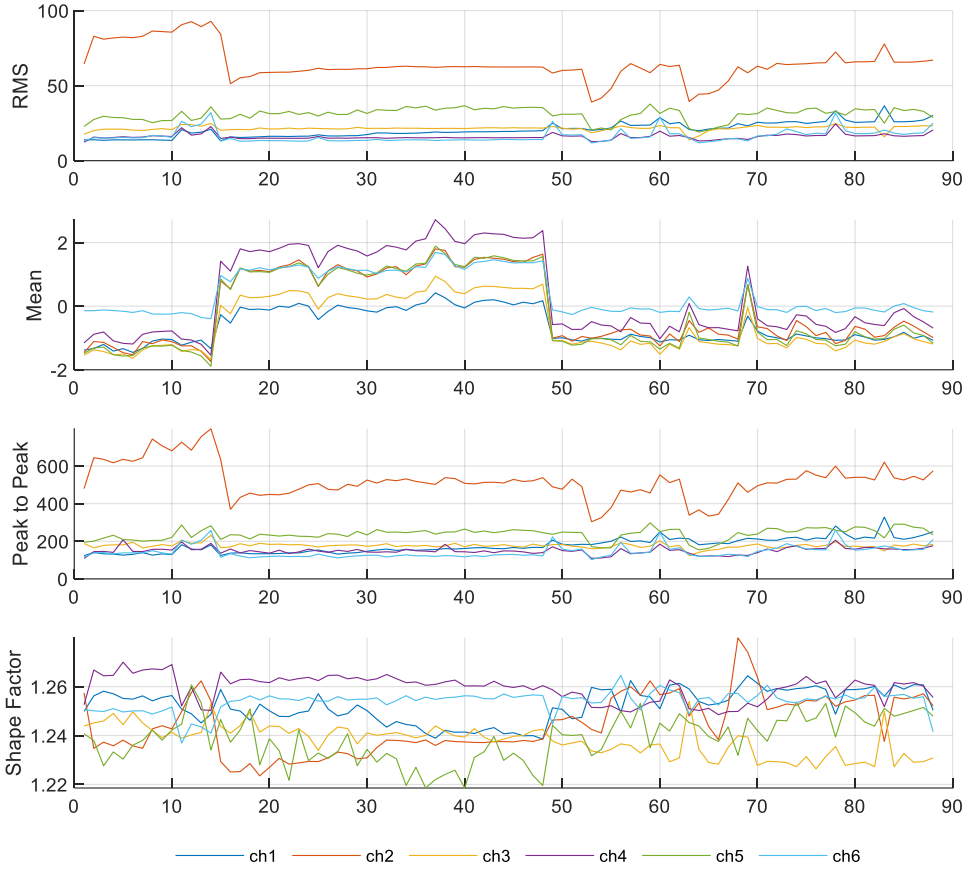

Figure 49: RMS, Mean value, Peak to Peak and Shape Factor computed on acquisitions every 4 test hours

In Figures 49 and 50, the features extracted from the vibrational signals relating to the 6 channels are represented. A first analysis can be done by evaluating the trend of the RMS parameter over time, as its values indicate the overall vibration of the system. With reference to the RMS value graph, the trend is almost constant and with the same amplitude for all channels except for channel 2, where a clear decrease in the RMS value is noted at a certain moment of the test, which then remains about constant. This is probably due to a settling phase of the system during running in, as the same trend can also be seen in the signals of the other channels, but of lesser importance. Effectively, at the same point also the average value changes significantly passing from only negative values for all channels to positive values. A trend similar to that of the RMS value is that of the Peak to Peak value, obtained from the difference between the maximum and the minimum value. These values are insensitive to signal impulsivity, therefore it is necessary to refer to the other features which are independent of the signal amplitude but depend only on the "shape" of the signal. An interesting comparison can be made

between the Shape Factor, Impulse Factor and Crest Factor parameters, which do not show significant variations between the start and end of the test. Also the graphs of the statistical parameters Kurtosis and Skewness have an almost constant trend, which indicate a normal and symmetrical distribution.

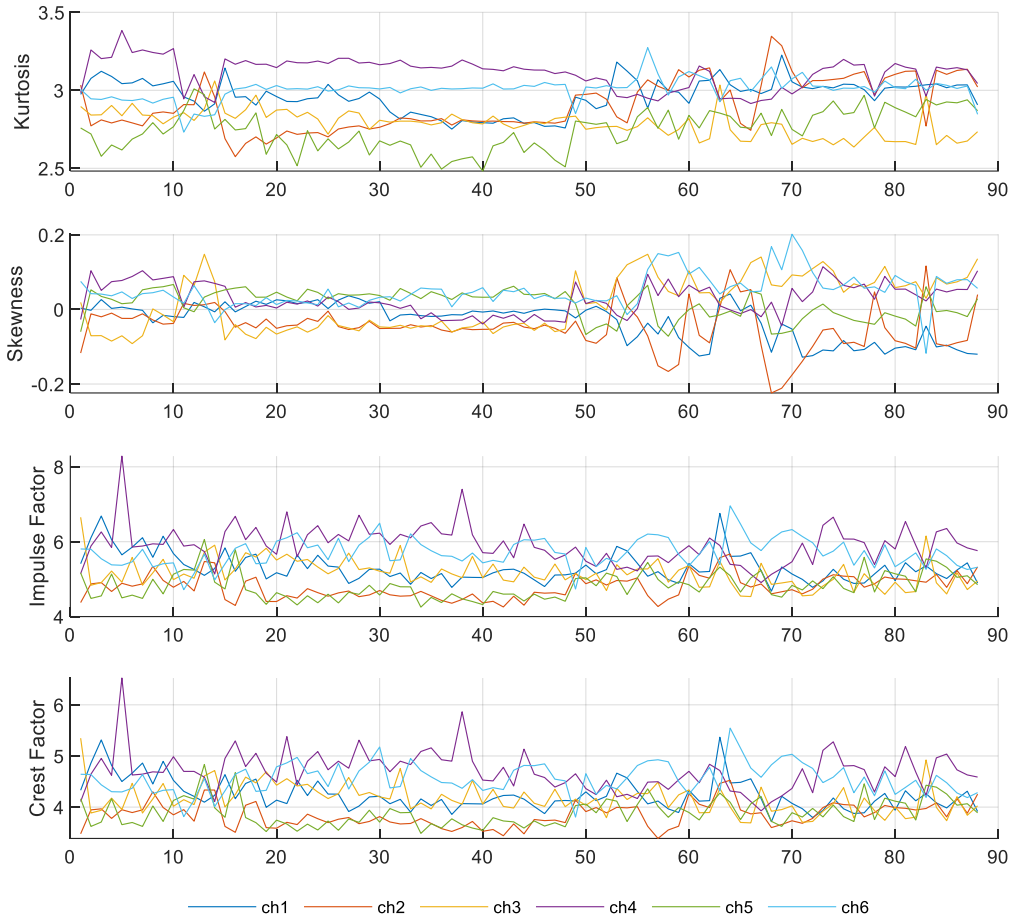

Figure 50: Kurtosis, Skewness, Impulse Factor and Crest Factor computed on acquisitions every 4 test hours

From this first analysis based on the features analyzed, it can be deduced that no anomalous trend has been identified and that therefore, considering the initial condition of new components, the end test condition does not present any index with representative values of a "damaged" component.

5.2.3. Bearings frequency detection

The procedure explained in chapter 4 has been implemented in *MATLAB®* and applied to the signals acquired during the endurance test. To demonstrate how the algorithm works, it is applied to the vibration signal acquisition, previously analyzed in time domain, with the purpose of identifying a damaged bearing. After extracting the residual non-deterministic signal (Last Residual), it is processed by the selected diagnostic algorithm for rolling element bearings.

A first analysis is done with the Fast Kurtogram algorithm. In this way, it's possible to identify the frequency band in which the signal shows the maximum kurtosis, i.e. where the signal is most impulsive. The algorithm can also bandpass filter the signal in that frequency band and provide a graphic visualization of both the filtered signal and its envelope spectrum. To check the bearing status during the test, the algorithm was applied to 10 acquisitions of vibration signal, performed with an interval of 50 hours of test running at the same operating condition of load – speed. The values obtained in terms of maximum value of kurtosis (K_{max}), level, bandwidth and center frequency (f_c) are displayed in the following table.

Acquisition n°	K_{max}	*level*	B_f [Hz]	f_c [Hz]
1	3.6	2.5	4166.67	22916.67
11	3.1	4.5	1041.67	23437.5
21	2.9	2.5	4166.67	22916.67
31	3.1	4.5	1041.67	23437.5
41	3	4.5	1041.67	23437.5
51	3.5	4.5	1041.67	23437.5
61	3.5	4.5	1041.67	23437.5
71	3.1	4.5	1041.67	23437.5
81	3.2	4.5	1041.67	23437.5
91	3.2	4.5	1041.67	23437.5

Table 15: Fast Kurtogram output comparison for acquisitions from 1 to 91

In the literature it has been demonstrated that the maximum level of kurtosis is low when the bearing is healthy, while a higher value is reached with damage to an element of the rolling bearing. As can be seen, in our case the maximum level of kurtosis remains almost stable, with small fluctuations around the values of 3 and 3.5. Another aspect that can be analyzed concerns the position of the f_c frequency in the frequency domain. It can be noted that for all the acquisitions this value is quite high (22000 - 23000 Hz) and concentrated in a narrow bandwidth (1000 - 4000 Hz). This reveals the algorithm's ability to detect and locate any impulsive transients in the analyzed signal. However,

even in this analysis, no important differences between the various acquisitions are found, especially in the last 7 acquisitions. This is in line with what has been seen from the analysis of the characteristics of the raw vibrational signals, since, apart from a few outlines, no important variation is noted, premonitory of a failure or progressive degradation.

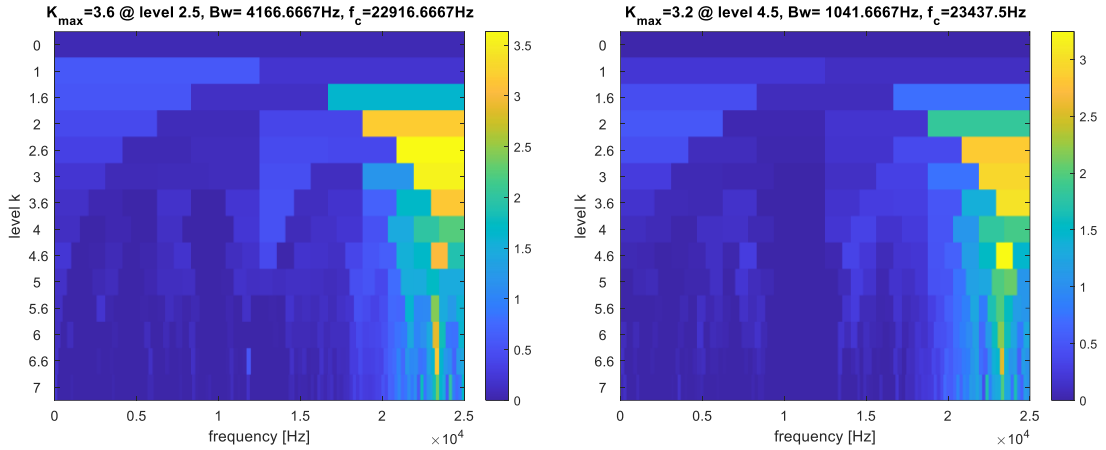

Figure 51: Fast Kurtogram evaluated for 8 seconds of acceleration of ch1 for acquistion n°: 1 (left) and 91 (right)

Once the frequency band with the highest impulsivity has been identified, the algorithm filters the signal in that band and calculates its envelope spectrum. The residual non-deterministic signal was also processed by the *Fast_SC.m* algorithm **(19)**, developed by J. Antoni to obtain the spectral coherence, able to detect the presence of cyclostationarity degrees in the signal and to identify the cyclic frequency of the defect in the bearing. For simplicity of analysis of the result, the axis of the cyclic frequency in both graphs has been referred to the orders of the input shaft; this makes it possible to visualize the characteristic frequencies of the defect in the bearings independently of the rotation speed of the different shafts.

Figures 52 and 53 show the envelope spectrum and the spectral coherence for acquisition n° 1, i.e. at the beginning of the endurance test, and for acquisition n° 91 at the end of the test. The dashed blue vertical lines spectrum graph indicate the characteristic frequency of the e-Axle bearings and the higher order harmonics. As can be seen from both envelope spectrum graphs, the broader spectral bands appear to coincide clearly with the BPFI of a bearing that supports the input shaft, except for small deviations. From a comparison between the initial and final acquisition, it is possible to note how the width of the spectral bands has increased over time, reaching a double value in the final spectrum compared to the initial one.

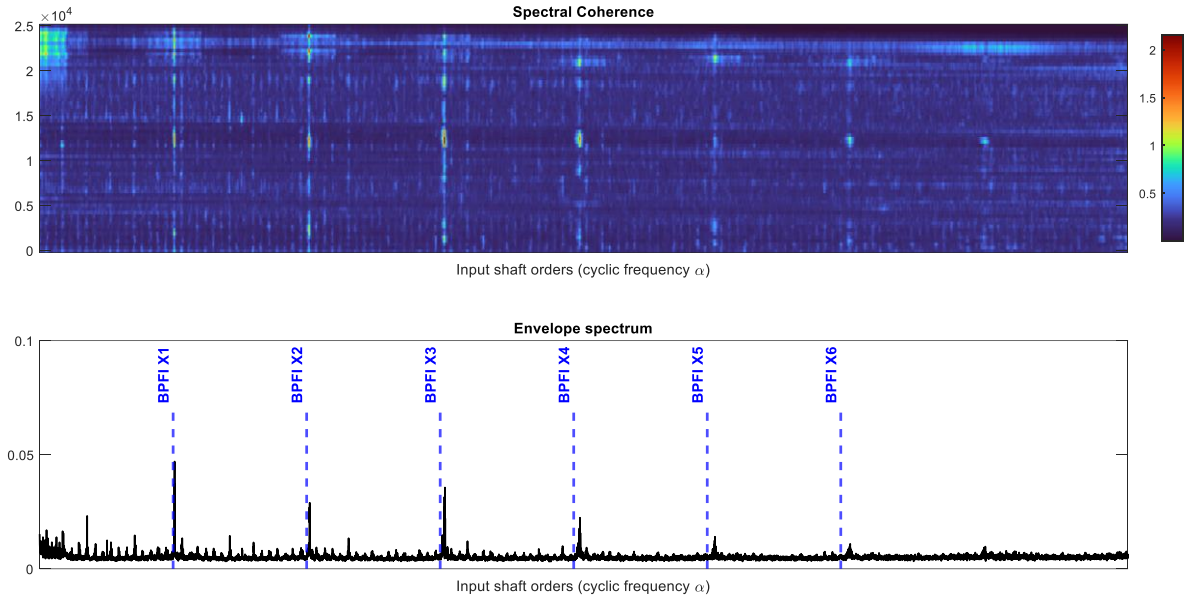

Figure 52: Spectral Coherence and Envelope spectrum for acquisition n° 1, ch1

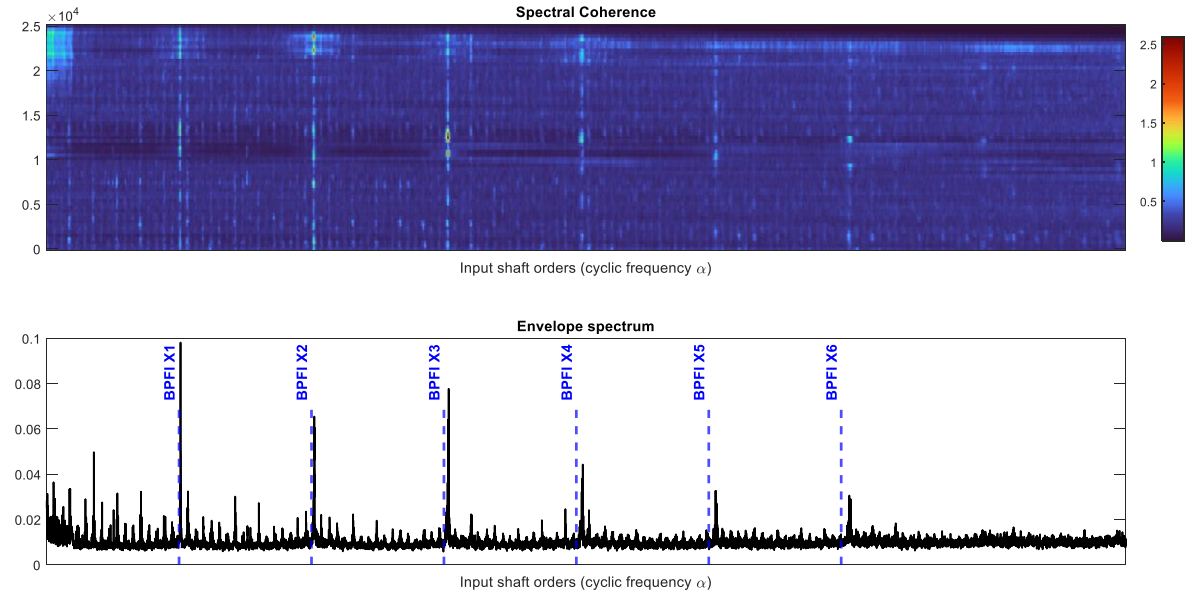

Figure 53: Spectral Coherence and Envelope spectrum for acquisition n° 91, ch1

In both Figures 52 and 53, the colormaps of the spectral coherence are shown, for a quick comparison with the envelope spectrum. It is easy to see that the same spectral bands with greater amplitude than all others, detected in the spectrum and related to the harmonics of the bearing BPFI stand out clearly in the colormap.

By deepening the analysis of the envelope spectrum, zooming into the area of the lowest orders, it is possible to notice that other bands with a smaller amplitude than the previous ones stand out quite evidently. Figure 53 show the correspondence for these orders with other characteristic frequencies of the e-Axle bearings for the acquisition n° 91 coming from the different channels. In particular, it is noted how the harmonics of the BPFI of the bearings that support the output shafts of the e-Axle stand out clearly, in particular those of even order. In addition, a spectral band matching exactly the FTF of another bearing supporting the input shaft, with no higher order harmonics, also emerges.

From the comparison between the spectra coming from the acquisitions of the different accelerometers, positioned in different locations on the e-Axle case, and from a comparison between them, it has however been found that there are very little differences between them. The only differences noted are related to the amplitude of the spectral bands, probably influenced by the power of the vibrational signal picked up by the various accelerometers and therefore by the distance of the signal source from the acquisition unit.

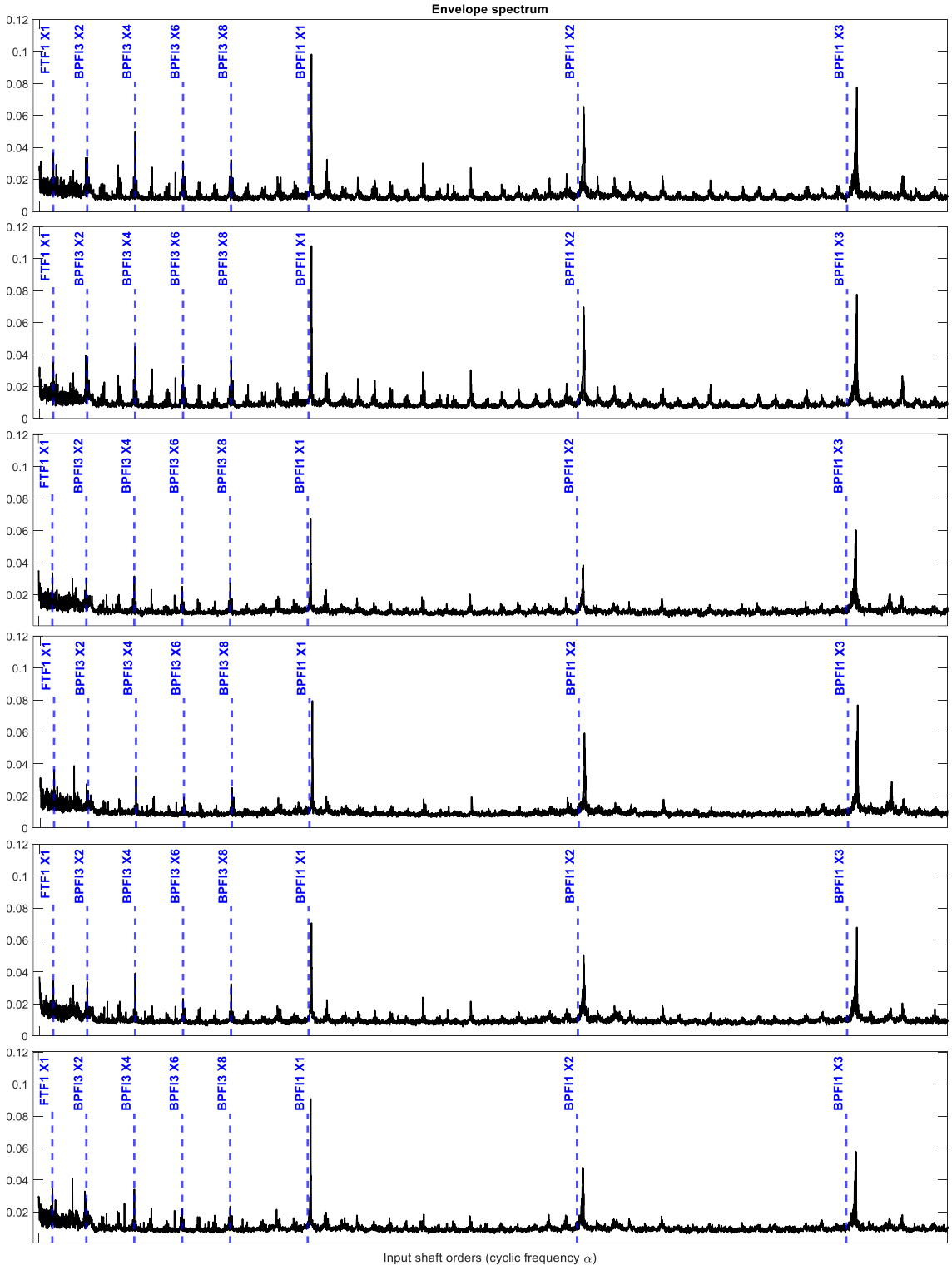

Figure 54: Zoom on the lowest orders in Envelope spectrum for acquisition n° 91, listed in order for the 6 channels (ch1-ch2-ch3-ch4-ch5-ch6)

5.2.4. Considerations and comparison between methods

Both algorithms used for rolling bearing diagnostics have proven efficient in extracting useful information from the non-deterministic residual signal. The Envelope Analysis, assisted by the Fast Kurtogram, allows the characteristic of the defect to be extracted in a clear and evident way in the form of spectral bands, which are distinguished by their greater amplitude than the others. By following the cyclostationary approach of the signal, the Spectral Coherence is able to extract eventual hidden periodicities in the residual signal and visualize them in the $\boldsymbol{f}, \boldsymbol{\alpha}$ plane. However, even in this case, the frequency of the defect in the bearing and the related harmonics are clearly delineated, but with some limitations due to the resolution of the image on the screen which prevents the detection of bearing frequencies at lower orders. Also, while those with greater amplitude stand out from the background, there are other spectral lines in the image that may cause difficulty in understanding.

By focusing on the comparison of the results obtained from the analysis between the beginning and the end of the test, several observations can be made. First of all, it can be said that the only aspect that seems to change is the width of the spectral bands, which doubles in the spectrum of the last acquisition (n° 91) compared to the first (n° 1). All the spectral bands identified in the last spectrum and correlated to a characteristic frequency of an e-Axle bearing appear in the spectrum of the first acquisition, but with a smaller amplitude.

By comparing the calculated BPFI frequency with that highlighted by the envelope spectrum, it is possible to note that there is a frequency offset between the two values which clearly increases in higher order harmonics. This deviation between real and theoretical values could be due to a variation of the contact angle between the raceways and the rolling elements during operation, caused by the variation of the local ratio of radial to axial load.

It is also important to note that, as previously mentioned, from the analysis carried out on the signal acquired by the various accelerometers, it can be deduced that the spectrum obtained is independent of their position on the e-Axle case, contrary to what was expected. This allows us to state that the identification of the spectral bands corresponding to a defect on a bearing, in the case analysed, is independent of the position of the transducer and therefore the transmission path covered by the modulated signal only affects the signal strength.

These observations allow us to draw some final considerations. The two algorithms applied to the acquired signals made it possible to identify some

characteristic frequencies of some bearings of the e-Axle, both in the spectrum of the initial signal and in that of the signal at the end of the test (acquisition n° 91), without substantial changes. Considering that the e-Axle had all new components at the beginning of the endurance test, what was found allows us to state that the results obtained from the vibration analysis most likely do not refer to defects in the bearings, but probably the modulation of the signal with these frequencies it is caused by other phenomena such as the frequency of passage of the rolling elements on the bearing rings. Furthermore, given that the detected frequencies remain the same throughout the test, the bearings should not exhibit any localized defects developed during the test.

These statements remain only hypotheses based on observation of the results, which should be validated with a detailed analysis of the components after disassembly of the e-Axle, verifying that they do not present any damage that could compromise their operation.

6. Conclusions and future developments

The purpose of the thesis was to define a bench endurance test for an e-Axle and subsequently the implementation of a method suitable for monitoring the component during the test from a vibrational point of view. The first step was the analysis of some vehicular missions representative of the life of the vehicle by investigating the aspects related to the cumulative damage caused by each of them according to the Palmgren-Miner theory. Once the vehicular mileage target was known, a test cycle was established with the number of repetitions necessary to have an equal damage with respect to the reference duty cycle.

Different signal processing and diagnostic algorithms proposed in the literature were investigated, in particular those aimed at analyzing damage in rolling bearings in rotating machines. The reference method, Envelope Analysis, supported by the Fast Kurtogram was firstly applied to signals with defects on the outer and inner races. The FK algorithm has proved to be simple to use and allows to quickly identify the band in which to filter the signal, where this shows greater impulsivity probably due to a damaged bearing. However, it has been highlighted that it is not always able to distinguish anomalous data from the raw signal and to identify the correct band, therefore it is necessary to evaluate whether the envelope spectrum is representative of the phenomenon.

From the literature it has been learned that the vibrational signal containing the signature of a bearing is contained within the overall vibrational response, but being much weaker than the vibrations caused by other rotating organs such as gears, it is hidden within the global vibration response. By exploiting the cyclostationary nature of these signals, different from the periodic one of the others, it is possible to separate the two contributions, isolating only the one necessary for the analysis of a possible damage in the bearings.

The signal processing techniques explored and implemented that have made it possible to isolate this contributions are Computed Order Tracking (COT) and Synchronous Average (SA). The combination of the two allows first to perform a resampling of the signal in the angular domain to give a specific and integer number of samples per period and an integer number of periods, then signal segments

corresponding to a complete rotation of the shaft must be averaged between them in order to eliminate any signal content that is not periodic. By identifying the periodic components for each shaft of the gearbox and applying the two algorithms in cascade, a procedure was implemented capable of obtaining the Last Residual signal automatically for all the accelerometer acquisitions made during the test.

Two analyzes were performed in parallel on the experimental data. A first-level one made it possible to monitor the trend during the test of some vibration indicators calculated on signal acquisitions performed at constant time intervals, while a more detailed analysis was conducted with the aim of identifying any characteristic frequencies of the bearings. The diagnostic procedure implemented in *MATLAB®* has been successfully applied to the various acquisitions, obtaining for each of them the Last Residual signal, purified of all deterministic contributions. At first, it was evaluated how the frequency band identified by the Fast Kurtogram and the maximum value of kurtosis vary over time, detecting practically zero variations between the start and the end of the test. Considered an acquisition corresponding to the beginning of the test and one at the end, both selected diagnostic algorithms were applied to the residual signal. Both the Envelope Analysis and the cyclostationary approach (Spectral Coherence) have proved capable of extrapolating from the residual signal the characteristic frequencies of some bearings that support the shafts of the gearbox. By comparing the spectra relating to the start and end of the test, it was concluded that being very similar, the frequencies identified probably hardly refer to localized defects in the bearings that arose during the test, considering that all the components at the start of the test were new. The characteristic frequencies of the bearings identified on the spectrum are probably due to various phenomena of a dynamic nature that cause the modulation of the vibrational signal, which would require further investigations.

Furthermore, by comparing the envelope spectrum resulting from the simultaneous acquisitions of accelerometers positioned in different points of the gearbox, it was possible to notice how they are really very similar to each other, with relative differences only in terms of spectral band width. It can be deduced that the position of the accelerometer with respect to the source is of little relevance for the purposes of identifying the characteristic frequencies, therefore the transmission path between the source and the transducer varies only the power of the detected signal.

Once the test is complete, the next step would be to check the state of wear of the components after complete disassembly of the e-Axle, highlighting any critical issues.

It would be interesting to verify the effectiveness of the proposed method in identifying any defects in rolling bearings during the test and observe their evolution over time, up to component complete failure. In this way, alarm thresholds could be defined, capable of automatically stopping the test, avoiding catastrophic failure. This could also highlight the difficulties of diagnostic algorithms in identifying distributed defects in rolling bearings, as in these cases the contact area becomes worn and the impacts could be much smaller than the early stages with localized defects.

The next step would be to implement the proposed procedure with the post processing and diagnostic algorithms directly on the acquisition software, with a specific calculation tool, to have real-time test control.

Figures index

Table index

Bibliography

1. ePowertrain. *FPT Industrial.* [Online] https://www.fptindustrial.com/it/products/ePOWERTRAIN/eDriveline/eAX-840-R.

2. Yuzhuo Men, Haitao Yu and Haibo Yu. Development of block loading spectrum for car powertrain rig test correlated with customers' usage. Advances in Mechanical Engineering, Vols. 2017, Vol. 9(9) 1–10.

3. *A New Dynamometer Test Rig to Develop Drive Lines for All-Wheel Driven Vehicles.* International, SAE. s.l. : Hans-Jürgen von Thun, Michael Pfeiffer and Louis Etschmaier, Vols. Vol. 97, Section 4: JOURNAL OF PASSENGER CARS (1988), pp. 1322-1334 (13 pages).

4. Lee, Yung-Li, et al. *Fatigue Testing and Analysis: Theory and Practice.* s.l. : Elsevier Science & Technology, 2004.

5. Randall, Robert Bond. *Vibration-Based Condition Monitoring : Industrial, Aerospace and Automotive Applications.* s.l. : John Wiley & Sons, 2011.

6. Daga, A. P. *Vibration Monitoring: Gearbox identification and faults detection.* s.l. : Politecnico di Torino, 2019.

7. *A review on signal processing techniques utilized in the fault diagnosis of rolling element bearings.* S.H. Upadhyaym, A. Rai. s.l. : ELSEVIER, 2016.

8. *Rolling element bearing diagnostics—A tutorial.* R. B. Randall, J. Antoni. s.l. : ELSEVIER, 2010.

9. L. Pascale, D. Marano, J. Langhart, S. Ebrahimi, T. Giese, U. Eiselt. Analisi e simulazione acustica di un assale elettrico. *Organi di trasmissione.* Novembre 2020.

10. Predictive Maintenance Toolbox - Signal Features. *Mathworks.* [Online] https://www.mathworks.com/help/predmaint/ug/signal-features.html.

11. Antoni, J. Fast Kurtogram. *Mathworks.* [Online] https://it.mathworks.com/matlabcentral/fileexchange/48912-fast-kurtogram.

12. *Cyclostationarity by examples.* Antoni, J. 2008, ELSEVIER.

13. *Cyclic spectral analysis in practice.* Antoni, J. s.l. : ELSEVIER, 2007, Mechanical System and SIgnal Processing.

14. *Analysis of computed order tracking.* K. R. Fyfe, E. D. S. Munck. 1997, Vol. Mechanical Systems and Signal Processing, pp. 187-205.

15. *A Review of Time Synchronous Average Algorithms.* E. Bechhoefer, M. Kingsley. 2009. Annual Conference of the Prognostics and Health Management Society.

16. *Feedback on the Surveillance 8 challenge: Vibration-based diagnosis of a Safran aircraft engine.* Antoni, Jérôme, et al. s.l. : Elsevier, 2017, Mechanical System and Signal Processing.

17. Dynamometer. *Wikipedia.* [Online] http://en.wikipedia.org/wiki/Dynamometer.

18. M., Pirra. *Advanced techniques for aircraft bearing diagnostic.* s.l. : Politecnico di Torino, 2013.

19. Antoni, J. Fast SC. *Mathworks.* [Online] https://it.mathworks.com/matlabcentral/fileexchange/60561-fast_sc-x-nw-alpha_max-fs-opt.

20. *A study on helicopter main gearbox planetary bearing fault diagnosis.* Linghao Zhou, Fang Duan, Michael Corsar, Faris Elasha, David Mba. 2019, Applied Acoustics, Vol. 147, pp. 4-14.

Acknowledgements

I would like to thank my thesis supervisor, Prof. Enrico Galvagno, for his constant availability and for providing me with useful advice in moments of indecision.
I thank Eng. Vincenzo Rombolà, my tutor at FPT Industrial company where I carried out this thesis work, for allowing me to have this experience that will be precious for my future and for immediately welcoming me into the team. I would particularly like to thank Eng. Domenico Netti for his absolute willingness to guide me in every phase of the thesis and above all, for having taught me so much in these months of experience. I will always carry with me the curiosity and desire to learn that you passed on to me. Thanks also to all the colleagues in the company for the extreme kindness and attention they have given me. I consider it a great fortune to have had the opportunity to carry out my thesis work in such an interesting and dynamic working environment.
Last but not least, I infinitely thank all my family, who have constantly supported and motivated me to give my best, and my closest friends, who have shared this university journey with me.